Langmuir Films of Graphene-Based Materials: Towards Large Area Monolayer Deposition

by

Luzhu Xu

A thesis
presented to the University of Waterloo
in fulfilment of the
thesis requirement for the degree of
Master of Applied Science
in
Chemical Engineering (Nanotechnology)

Waterloo, Ontario, Canada, 2017

AUTHOR'S DECLARATION

I hereby declare that I am the sole author of this thesis. This is a true copy of the thesis, including any required final revisions, as accepted by my examiners.

I understand that my thesis may be made electronically available to the public.

ABSTRACT

Graphene-based materials have attracted considerable interest due to their potential use in a broad range of applications including membrane separations, electronic devices and biomaterials. Their performance in many of these applications relies on the ability to precisely control the layer number and density of films over large areas. Chemical vapor deposition (CVD) is one of the most promising methods to produce single layer graphene. However, the high cost, limited choice of substrates and error-prone transfer processes limit its application. On the other hand, laboratory-scale film processing approaches like spin/spray-coating, filtration and drop-casting are incapable of producing films with nanometer-scale control of film thickness and uniformity and/or over the large length scales required for many applications. Recently, the Langmuir-Blodgett (LB) deposition technique has been applied to graphene and graphene oxide with some success. In this method, the material is dispersed at the air-water interface, the floating material, held up by surface tension, is densified by the compression of two floating barriers and the resulting film is transferred onto substrates by dip coating. While good control over layer number and film density has been achieved, the technique is currently limited to small area films and suffers from the challenge that only ~1% of the material is retained at the interface during transfer while the rest is lost in the sub-phase. In this work, we developed a directed assembly process for producing GO monolayers at the air-water interface which assemble into densely tiled films without the requirement to use adjustable barriers. We demonstrate that the resulting directional film growth is amenable to roll-to-roll fabrication. By choosing a suitable spreading solvent, we obtained high-yield transfer to the air-water interface measuring Langmuir surface areas as high as 800 m^2/g. Furthermore, we used both *in situ* Brewster angle microscopy and a custom-made Langmuir-Adam balance to study the mechanism of film formation. We also successfully extended our process to monolayer films of other 2D nanomaterials such as MoS_2. As a first example of the utility of these films, we deposit dense GO monolayers onto silver nanowire transparent electrodes and demonstrate their ability to protect the nanowires from degrading under high currents.

ACKNOWLEDGEMENTS

I would first like to thank my supervisor Dr. Michael A. Pope for guiding me through my Master's studies. His patience, motivation and enthusiasm to research have had a big impact on my studies. I deeply appreciate his guidance and patience while I was writing my thesis, in addition to helping my written English. I would also like to thank Dr. Shawn Wettig and Dr. Boxin Zhao for being on my committee. I would again like to thank Dr. Shawn Wettig for letting me use his Langmuir-Blodgett trough and Brewster angle microscope as well as Dr. Juewen Liu for letting me use his Zetasizer instrument. I would also like to thank Dr. Irene Goldthrope and Dr. Hadi Hosseinzadeh Khaligh for their contributions in our collaborations. Last but not least, I would like to thank my lab mates and my friends for their support throughout my masters.

Finally, I would like to thank my parents for their unwavering support while I'm pursuing my graduate studies in Canada.

DEDICATION

Dedicated to my Family

TABLE OF CONTENTS

LIST OF FIGURES

LIST OF TABLES

LIST OF ABBREVIATIONS

GO	Graphite oxide
rGO	Reduced graphene oxide
TEGO	Thermally exfoliated graphene oxide
DCE	1,2-Dichloroethane
AFM	Atomic force microscopy
BAM	Brewster angle microscopy
LB	Langmuir-Blodgett
LSSA	Langmuir specific surface surface area
SSA	Specific surface area
AgNW	Ag nanowires
IR	Infrared
2D	2-dimensional
SEM	Scanning electron microscopy
ITO	Indium tin oxide
OLED	Organic light emitting diode

1 Introduction

Since the 1920s, the Langmuir-Blodgett (LB) deposition technique has proven to be one of the most controlled approaches for depositing films only one molecular layer thick. Classically, insoluble amphiphiles were used to create these well-ordered thin films, by one or more deposition steps. Nowadays, the technique is being used increasingly to deposit a variety of nanomaterials including graphene and graphene oxide (GO) onto a wide array of substrates. [1–6]

In particular, thin films of graphene and related 2D materials have attracted considerable interest due to their potential use in a broad range of applications which include flexible and/or transparent electronic devices,[7–13] molecular blocking layers,[14–16] and selectively permeable membranes.[17–19]

For example, LB films of micron-sized graphene oxide single layers have been used to prepare transparent conductors with optical conductivities approaching those of films grown by high vacuum, high temperature vapor deposition methods (e.g., CVD) while significantly outperforming films deposited by more common solution processing techniques such as vacuum-filtration,[13,20] spay-coating,[21] spin coating[22,23] or electrophoretic deposition[24] which result in less uniform thin films with either lower bulk density or lower transparency.

The LB process involves spreading a volatile, water-immiscible solvent, containing the material to be deposited, at the air-water interface of a water-filled trough. Evaporation of the solvent leaves any insoluble material floating at the air-water interface. Movable barriers are then used to compress the floating material to the desired density while measuring the surface tension (γ) or surface pressure ($\pi \equiv \gamma_{\text{water}}$-$\gamma$). The resulting film is then transferred to a substrate, typically by dip-coating, and the process can be repeated until the floating film is used up. Using this method, monolayers of graphene-based materials with area coverages upwards of 95%[1,8] can be made and transferred to substrates to create dense, robust thin films and heterostructures.

While promising, the LB approach has a critical drawback which limits its commercial application. Compressed, floating films are typically 1/5th the area of the trough which limits how much material can be deposited onto a substrate in one batch. While typical trough set-ups are only capable of coating substrates ~cm^2, recently, trough designs incorporating roll-to-roll coating equipment have been demonstrated.[25] However, the amount of material deposited is still limited by the film area enclosed by the moveable barriers used to densify the floating film. Ideally, film transfer would be coupled to continuous material deposition to make the process truly roll-to-roll.

This limitation stems from the belief that floating materials must be well-dispersed at the air-water interface. In the case of graphene oxide, it has been shown that a repulsive electrostatic force exists between the floating sheets which allows them to be densified uniformly and reversibly.[1] In the traditional case of insoluble amphiphiles, the relatively strong thermal motion and only weak attractive forces enable films to reversibly traverse gas, liquid and solid phases upon compression/expansion of the barriers.

However, for the case of graphene oxide, the process has been complicated by the fact that water-miscible spreading solvents are used due to the ease in which GO is dispersed in water and other polar solvents. Spreading such solvents at the air-water interface causes extensive mixing and results in the loss of up to 99% of material into the water-sub-phase[26] and has been shown to result in mostly the largest sheets selectively accumulating at the air-water interface.[27] This problem of poor transfer efficiency was recently addressed by Nie *et al*. by spreading nanoparticle dispersions using aerosols instead of macroscopic drops in order to minimize the mixing.[28]

Until recently, it was thought that GO could only be dispersed as single sheets in water and other polar solvents.[29,30] If fact, in as early as 1992, observations of the conformation of graphene oxide (presumably single layers – although not proven at that time) in water/acetone mixtures indicated that GO would form a crumpled or collapsed conformation in dilute solution (> 10% acetone). [31] However, while this may be the case under certain conditions, Lee's group has recently demonstrated the ability to effectively disperse GO as single sheets in a mixture of NMP with different nonpolar organic solvents, only as a low content in the mixture, including 1-butanol, tetrahydrofuran and dichloromethane.[32]

Therefore, in this work we will first present a method which enables high-yield transfer of GO onto the air-water interface by formulating dispersions in water immiscible solvents, like 1,2-dichloroethane and chloroform. We will then introduce a barrier-free deposition approach which is able to densify large area monolayer GO films during both batch deposition and by continuous deposition and withdrawal. We will also demonstrate that this approach can be extended to other 2D materials such as thermally exfoliated graphite oxide (TEGO) and chemically exfoliated molybdenum disulfide (MoS_2). The mechanism of film densification and aggregation are also investigated in an attempt to understand and thus control our process. Lastly, we will present the performance of our monolayer GO film in one particular application – a passivation layer to preventing silver nanowires from degrading under current flow.

2 Background

2.1 Graphene-based materials

Graphene, a single atomic layer of sp^2 bonded carbon atoms, is a promising material for many applications.[33] It was first discovered by mechanically exfoliating a graphite crystal using Scotch™ tape in 2004.[34] However, this method is not effective for large-scale manufacture of single layer graphene. On the other hand, chemically oxidizing graphite flakes to graphene oxide (GO) has emerged as a more practical approach for producing graphene-based materials in large scale.[35–38] GO can be easily dispersed in water as single layers and then chemically or thermally reduced to remove the oxygen-containing functional groups and restore the sp^2 hybridized network of graphene.[29,39] However, this conversion is incomplete leaving residual functional groups and carbon vacancies which act as defects in the graphene lattice. Therefore, to differentiate this material from pristine graphene, it is often referred to as reduced graphene oxide (rGO). The functional groups on GO and that remain, to some extent, on rGO consist of mostly hydroxyl and epoxide groups on the basal plane and phenolic hydroxyls and carboxylic acid groups at the edges. The presence of these functional groups increases the interlayer spacing from 0.335 nm for graphite to more than 0.625 nm for GO.[40] The hydrophilicity imparted by the functional groups on GO allow it to be dispersed in water as single sheets

[29] and in some polar solvents[30,32]. The phenolic hydroxyls and carboxylic acids at the edges can be deprotonated leading to strong electrostatic repulsion with the most stable dispersions around a pH~10 where the zeta potential is -40-60 mV. Depending on the chemical or thermal reduction process used to convert GO to rGO, the resulting rGO can achieve a C/O ranging from about 1.6 for GO to ~400 after high temperature treatment [35,40–42]. In this way the conductivity and degree of functionalization can be tuned.

2.2 Thin film formation strategies

Graphene-based thin films have been used in various applications especially as transparent conductors, the performance of which is highly related to uniformity and film density. Chemical vapor deposition (CVD) is one of the most promising methods to produce single layer graphene films.[11,43,44] However, the high vacuum, high purity and high temperature conditions make such films costly. There also exists only a limited number of growth substrates for graphene by CVD which requires error-prone transfer to other substrates for use in applications. Other methods such as vacuum-filtration[13,20], spray-coating[21], spin coating[22,23], electrophoretic deposition[24] and Langmuir-Blodgett (LB) assembly[1–6] have also been utilized to fabricate transparent conductive thin films from graphene-based materials. However, the main challenge in all of these approaches, except LB assembly, is their inability to produce films with nanometer-scale control of film thickness and/or uniform coverage over large length scales. These techniques are more suited to apply micron thick films.

2.3 Langmuir films and the Langmuir-Blodgett technique

2.3.1 Langmuir films of insoluble amphiphiles

In 1773, Franklin observed that the water wave in the pond calms down by only placing a teaspoon of oil on the pond indicating that the oil spread out as a film covering a large area of water surface. A century later, Rayleigh observed an apparent decrease in surface tension when sufficient amount of olive oil was deposited on a limited water surface. Based on his observation, he was able to calculate that the thickness of the spreading monolayer was around 1.6 nm by the volume of oil and the covered surface area. A more controlled method of studying the spreading of insoluble monolayers at the water surface was developed by Langmuir in the early 1910s. The studied insoluble oils were amphiphilic, meaning that the molecules are composed of two parts: a hydrophilic head, which is water-soluble, as well as a hydrophobic tail, which is water-insoluble. Thus, when these molecules are spread at the air-water interface, the hydrophilic head interacts preferentially with water while the hydrophobic tail prefers the air. The amount of insoluble amphiphile needed to deposit a monomolecular layer is so minute that it is usually dissolved in a volatile spreading solvent and several hundred microliters of such a solution is injected onto the air-water interface. The change in surface tension affected by the insoluble layer can be measured and is often reported as a surface pressure defined as $\pi = \gamma_0 - \gamma$ where γ_0 is the surface tension of pure water. The surface pressure can be thought of as the 2D analogue to pressure in the 3D world. The surface pressure can be adjusted by compressing the insoluble film which changes the interfacial area covered by the amphiphile. Langmuir and

Blodgett developed a technique, called Langmuir-Blodgett (LB) assembly, in which the surface pressure can be monitored and controlled while the resulting monolayer can be transferring onto solid substrates successively by dip coating. A schematic illustration of the equipment setup is shown in Figure 2.1 In a typical deposition, first of all, a small amount of amphiphiles are transferred onto spreading area. Then, by closing the barriers from the two sides slowly, the surface pressure is observed to increase as the molecules are squeezed closer together. 2D phase transitions are also evident in these systems which can traverse the gas, liquid and solid phases during film densification. Compression beyond the solid phase can cause the monolayer to collapse. To transfer a dense monolayer film to a substrate, the film is usually compressed to the solid phase and the surface pressure maintained by the barriers while a substrate is dip-coated, as shown in Figure 2.1c. This process can be repeated to build up a film layer-by-layer.

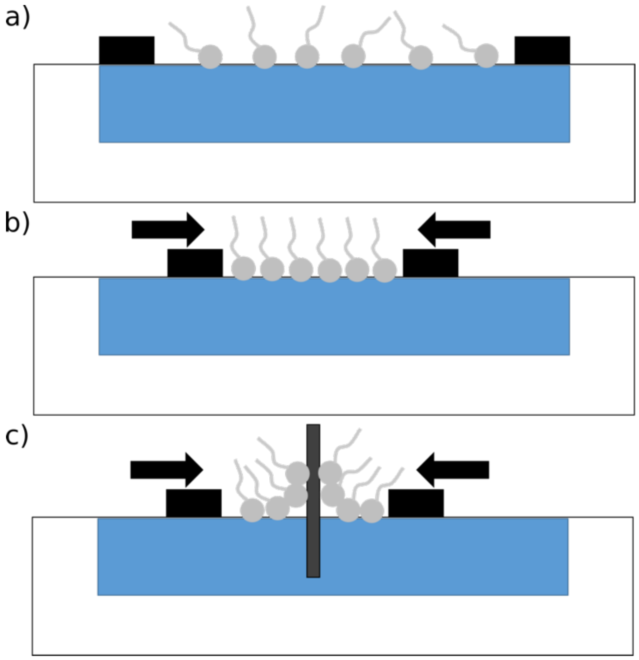

Figure 2.1 Schematic illustration of Langmuir-Blodgett assembly of amphiphiles

2.3.2 Langmuir film of nanomaterials

Many lightweight materials float on water (e.g., leaves on a pond) even if they are denser than water itself. They are held afloat by surface tension. This phenomenon also occurs with nanoparticles which can be dispersed at the air-water interface by spreading them onto the interface from a volatile spreading solvent (in a similar fashion to traditional small molecule Langmuir films). In this way, the LB technique has been used to fabricate monolayer films of gold, silver nanoparticles,[45,46] CuPc nanoparticles,[47] as well as carbon nanotubes.[48–50] In 2008, Cote *et al.*, demonstrated that this technique could be used to create single layer films of GO. In their typical process, GO sheets were dispersed in water/methanol mixture with a volume ratio of 1:5. Then the suspension carrying GO sheets was spread at the air-water interface. This process was found to leave the sheets floating on the water. After the desired amount of suspension was added onto the water surface, the sheets were densified by compressing the movable barriers. Compared to spreading films of lipids, in which only ~20-100 μL of spreading solvent needs to be injected by syringe, for GO deposition several to several tens of milliliters of solvent have to be dripped onto the water surface. This requires repetitive dripping onto the water surface by syringe pump instead of simply adding several drops of dispersion from a micropipette or micro-syringe. While seemingly inconsequential, we will show that this changes the Langmuir deposition process considerably. After addition of GO, closing the barriers resulted in the formation of a close-packed array of tiled graphene oxide sheets when the surface pressure is increased to ~10-15 mN/m, as shown in Figure 2.2b.[1] However, winkles as well as overlaps could be induced when higher surface pressures were employed (Figure 2.2d). As the hydrophilicity of GO can be tuned by the degree of ionization of the carboxylic acid group through pH, Cote *et al*. suggested that more wrinkling behaviors were observed in acidic subphase due to larger amount of unionized carboxylic groups at the edges leading to hydrogen bonding between the sheets (Figure 2.3a), while overlaps were observed in the high pH case where sheets are hydrophilic due to the more ionized carboxylic groups and water serves as a lubrication layer to allow sheets slide over each other (Figure 2.3b).[51]

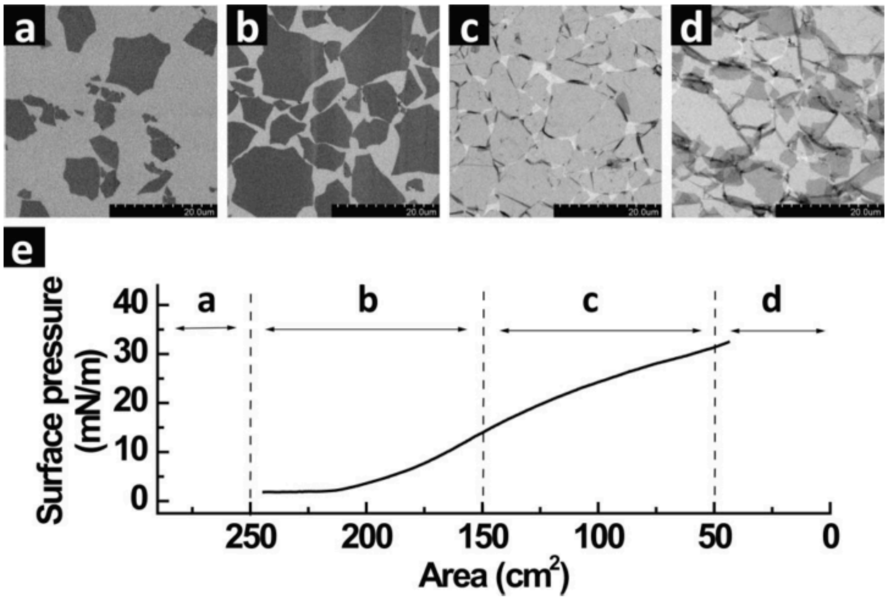

Figure 2.2 Langmuir-Blodgett assembly of GO monolayers. SEM images (a-d) show the collected graphite oxide monolayers on a silicon wafer at different regions of the isotherm. Reproduced from [1]

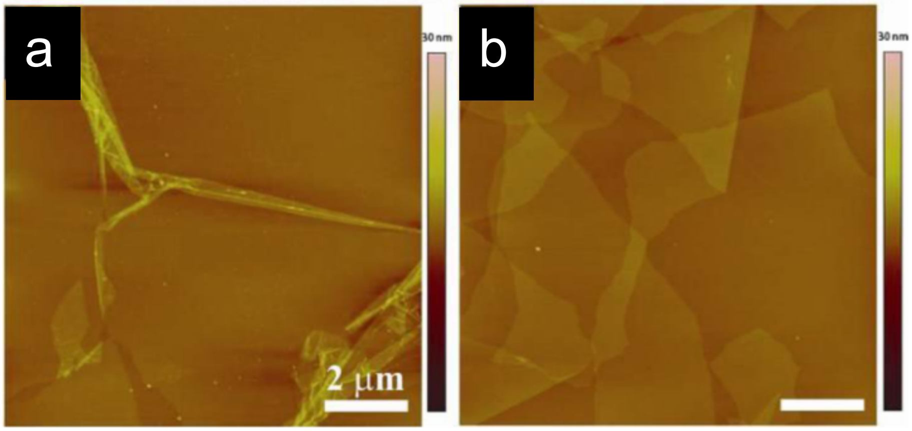

Figure 2.3 AFM images of LB assembly GO thin films prepared over various pH subphase: (a) acidic subphase and (b) basic subphase. The scale bar in a is valid in b as well. Reproduced from [51]

While promising, there are still some problems with LB assembly of GO monolayers. First, it has been reported that 99% of the sheets are lost in the subphase water.[26] Cote *et al.* also found out that, GO sheets with small sheet size are more likely sink into the sub-phase while the large sheets are observed to float on the water.[52] The spreading solvent, which is a mixture of methanol and water at a volume ratio of 5:1, is responsible for this loss of materials since the dispersion is completely miscible with water. Although researchers have since attempted to use other spreading solvents, these solvents are still totally miscible with water. Their works are summarized in Table 1 and this is likely due to the believe that GO sheets can only be will-dispersed in water and some polar solvents.[29,30] Recently, Nie *et al.* developed a new spreading approach – electrospray, which resolved high-yield transfer efficiency by decreasing the drop size.[28] However, from their microscopy images it was clear that many small-size droplets spread at the same time and caused uncontrolled overlaps between sheets during the deposition. Another limitation of the current LB technique is that the size of resulting film produced by traditional LB assembly is limited by the available coating area between the two movable barriers. Li *et al*. introduced a continuous coating bath by removing the barriers, depositing the materials onto water surface via repetitive dripping and densifying the film by inducing water flow in the sub-phase.[53] The shear on the monolayer induced by the flowing water has enabled control over the densification of nanoparticles to create large area colloidal crystals.

Table 2.1 Solvents used for spreading GO sheets at the air-water interface

Spreading solvents	References
water-ethanol (1:5)	[1], [54], [4], [51], [3], [2]
water-ethanol (1:9)	[26]
water-2-isopropyl alcohol (1:1)	[55]
water-acetone (1:5)	[6]

2.3.3 Liquids spreading on one another

As we discussed in §2.3.2, unlike amphiphiles, several to several tens of milliliters of spreading solvent is required to transfer sufficient amount of nanomaterials onto the air-water interface and in our barrier-free densification approach, the film is likely densified by lateral pressure from solvent spreading. Therefore, understanding the nature of a liquid spreading on another liquid is quite essential in our work. On the molecular level, the molecules in the bulk are surrounded by nearest neighbours and form many interactions which lower the system energy. However, the molecules at an interface are missing some of these interactions as they directly contact air or vacuum (in the case of the air-water interface) or a solid or liquid which puts the system into a higher energy state due to the presence of an interface. This change in energy can be accounted as the work required to move molecules from the bulk to the surface to create new interfacial area. The work is defined as surface energy or interfacial tension, represented as γ in a unit of mN/m.

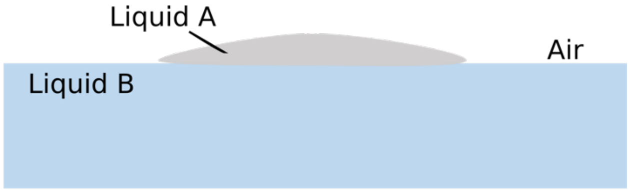

Figure 2.4 Schematic illustration of liquid A spreading at the surface of liquid B

When an upper liquid (A) contacts a lower liquid (B), the liquid-liquid interface (AB) replaces the A-vapour and B-vapour interfaces (Figure 2.4). However, this will only occur spontaneously (i.e., liquid A will spread on liquid B) if there is a decrease in the free energy of the system. Thus the criteria of spreading is that $\gamma_{av} + \gamma_{ab} - \gamma_{bv} < 0$. This is typically quantified by the spreading coefficient $S = \gamma_{bv} - \gamma_{ab} - \gamma_{av}$ which must be positive. The cohesion of a liquid is defined as the work required to separate a volume of unit cross-sectional area in the liquid, while adhesion between two liquids is determined by the work to separate two immiscible liquids to create two new interfaces. Thus, one could expect that the adhesion between upper and lower liquids must be greater than the cohesion of the upper one if spreading occurs. Note that water is chosen as the lower liquid in all our experiments.

While the sign of S tells us if spreading will occur, its magnitude tells us something about the driving force for spreading. However, the dynamics of spreading are dictated by kinetic factors such as the viscosity of the two liquids as well as the evaporation rate. A spreading front encounters resistance from fluid movement induced by the spreading and evaporation processes. For example, Harkins observed that spreading could occur rapidly even for liquids with a relatively small S.[56]

When a small volume of liquid A spreads on the surface of water, the initial spreading movement of liquid A is mainly due to gravity. When the film is thin enough that gravity no longer plays a role, the interfacial tension starts to dominate the spreading process. Generally, as shown in Figure 2.5, a spreading film can be divided into three regions: reservoir (liquid source) at the center, boundary, a monolayer or submicron thickness of spreading film, the leading edge, the spreading front.[57] Therefore, the movement of spreading liquid will be mainly due to the gravity force in the reservoir region where the spreading liquid is initially placed. At the edge of the spreading film, the gradient of the interfacial tension at the boundary dictates the force, given by: [57]

$$\mu_w \left.\frac{\partial u_w}{\partial z}\right|_{z=0} = -\frac{\partial \gamma}{\partial x}$$

where μ_w is the viscosity of water, u_w is the horizontal velocity component of water , z and x are the vertical and horizontal co-ordinates at the interface with $z = 0$ as the approximate location of the interface of two liquids. This force is called the Marangoni effect. The γ represents the overall tension of the film plus the water surface and is correlated to the spreading force acting at the spreading front. Its value is related to the thickness of the film in the boundary. If the film is a monolayer, γ is the sum of $(\gamma_A + \gamma_w)$, where γ_A and γ_w represent the surface tension of spreading liquid and water respectively. However, if the film is thicker, γ will change as a function of film thickness. So far, the spreading mechanism discussed is only applied to the case where non-volatile, water-immiscible solvents, such as silicon oil, spread at the water surface.

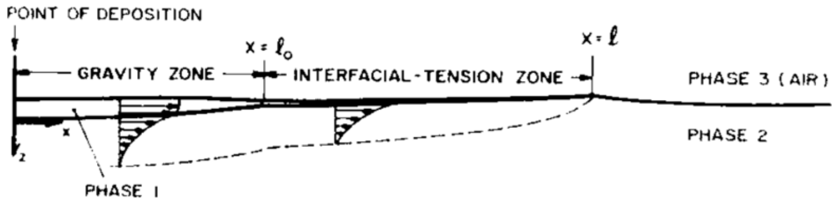

Figure 2.5 Schematic illustration of three regions when liquid 1 spreads at the surface of liquid 2. Reproduced from [57]

In the case of creating Langmuir film at the air-water interface, which will be discussed in later sections, a volatile organic solvent is used to transport materials onto the air-water interface, which evaporates completely from the water surface leaving no residue. Thus the understanding of spreading kinetics of solvent coupled with evaporation is necessary for producing uniform monolayer Langmuir film at water surface. Davies and Rideal reported a decrease spreading rate by studying the spreading of ethanol and acetone at the water surface, which they believe is due to the depletion of spreading film by evaporation.[58] Dussaud *et al.* studied the spreading movements of various volatile solvents including toluene, *p*-xylene, trimethylpentane, as well as *n*-heptane using laser shadowgraphy showing the same result and suggested that Maragoni driven spreading in the presence of evaporation shows a less aggressive spreading movement which they attributed to the presence of a convective roll induced by spreading and evaporation in the sub-phase water underneath the spreading front.[59]

2.3.4 Applications of LB GO/rGO films

LB GO/rGO films have been successively used in various applications since 2008 especially in electronic devices. Lin *et al.* fabricated conductive transparent films by layer-by-layer deposition of LB GO films onto substrates. The electrical performance of the resulting film after reduction of GO to rGO and chemical doping can achieve as high as ~1100 Ω sq^{-1} at 91% transmittance.[6] Jia *et al*. assembled sulphonated rGO sheets into densely-packed monolayers by LB deposition and confirmed that the as-prepared rGO film exhibited ultrahigh capacitance and excellent cyclic stability.[60] Moreover, Yang *et al*. demonstrated that their LB rGO film was able to serve as a hole injection layers for an organic light-emitting diode with a better luminance performance due to higher hole carrier injection efficiency compared to a commercial conducting polymer PEDOT:PSS.[61] Liu *et al*. demonstrated the utilization of LB rGO film as nitric oxide sensor which exhibited high sensitivity and low detection limit.[62]

2.4 Measuring surface pressure of Langmuir films

2.4.1 Langmuir-Adam balance and the measurement of spreading pressure

The Wilhemy plate technique is the most common method to measure the surface pressure. A thin plate of filter paper or platinum is placed at the interface and the force of surface tension exerted on the plate is determined by a tensiometer. However, this method requires the contact angle between the liquid phase and the plate to be zero. Since in our case we would like to study the surface tension during deposition, the plate would be in contact with non-aqueous spreading solvents and the air-water interface will be disturbed by dripping making the Wilhelmy plate approach not ideal. On the other hand, the so-called Langmuir-Adam balance was also developed to measure the surface pressure of insoluble monolayers at the air-water interface over a century ago.[63] A brief schematic of the equipment setup is shown in Figure 2.6. The balance was initially built up by Langmuir and modified by Adam. A large copper dish having flat waxed edges was filled with water. The top-view is shown in Figure 2.6a. Two metal strips B and D were used to sweep over the water surface so as to clean out the contaminations. The balance was placed on one side of the dish while another metal strip C, which could be used to compress the floating film, was on the other side. A light floating barrier was attached to a rod and then to the torsion wire, as shown in Figure 2.6b. The floating material was spread between C and D and the pressure/force exerted by film was measured as the rotated degree of the torsion wire. A clean water surface area must be guaranteed behind the floating barrier which would move according to the difference of surface tension at the front and back of the float. Note that the accuracy of the measurement is highly impacted by the cleanness of the water surface between the floating barrier and strip D. The floating barrier was made to be narrower than the width of the dish so that it could move freely. However, the space between floating barrier and sides has to be filled up to prevent the floating material from leaking behind the float. Langmuir used an air jet to block molecules from leaking. However, this disturbed the floating monolayers and induced large error in the final measurements. Adam added thin ribbons of metallic leaf coated with wax at the two ends of barrier to join it to the edges, which highly improved the accuracy as well as reproducibility. He also added one more torsion wire close to the floating barrier and was able to increase the accuracy of the measurement to 0.01 mN/m.

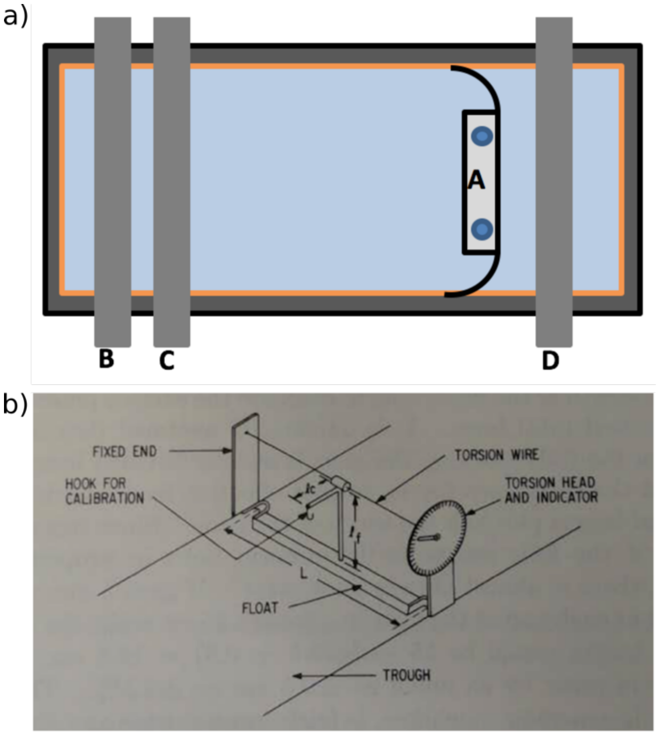

Figure 2.6 Schematic illustration of Langmuir-Adam balance set up. Top view of the setup without balance (a). Schematic illustration of a Langmuir balance using torsion-wire. Reproduced from [63]

In terms of measuring the surface pressure by the Langmuir-Adam balance, a desired amount of floating materials is transferred onto the water surface and the materials is compressed by a movable barrier on the other side of the float. The force acting along the float is interpreted as the surface pressure of the film.

Transue *et al.* developed a simple method to directly measure the spreading pressure of volatile solvents using the Langmuir-Adam balance.[64] A monolayer of stearic acid was deposited on the water surface to produce an initial surface pressure by compression of the movable barrier. Then a few drops of volatile solvent spread at the surface which exert pressure on the monolayers thus causing an increase in surface pressure. This final surface pressure was constant over a wide range of initial pressure and was taken to be the spreading pressure of the volatile solvent.

2.5 Goals and layout of thesis work

The main goal of this thesis is to develop a methodology, which is scalable and inexpensive, to create and deposit large area monolayer films mainly from graphene-based materials as well as other water-stable 2D materials.

Specific aim 1 – Improve the transfer efficiency of GO single layers onto the air-water interface

Specific aim 2 – Develop a deposition approach to enable deposition of large area monolayer films of GO in a continuous manner

Specific aim 3 – Study the film formation mechanism in the developed deposition approach

Specific aim 4 – Investigate the potential of extending the densification method to other 2D materials

Specific aim 5 – Demonstrate the concept of developing this deposition method into continuous coating process

Specific aim 6 – Investigate the utility of the resulting GO film in one application to demonstrate the uniformity of film density and thickness.

In §3, I will present a method to achieve high-yield transfer efficiency of GO sheets onto the air-water interface achieved by using a new spreading solvent which is mostly immiscible with water. I will then introduce a barrier-free deposition method which is able to direct the assembly of large-area films, up to 204 cm^2. The concentration and sheet-size effect on the resulting films is also studied. Moreover, in this chapter I will also discuss the aggregation phenomenon of floating GO sheets we observed during the film formation by barrier-free deposition. As we observed the film densified regardless of concentration and pH conditions, we hypothesized that the spreading pressure from solvent spreading is responsible for the densification. Therefore, in §4, I will investigate the mechanism of spreading-induced film densification by measuring the spreading pressure of solvent during deposition using a custom-made Langmuir-Adam balance. In §5, I will present preliminary results demonstrating large area Langmuir film of other 2D materials such as MoS_2 and thermal exfoliated graphene oxide (TEGO) by using our barrier-free deposition. In addition, I will also present a coating result of long strip of PET with continuous TEGO film to demonstrate the concept of developing our approach into a continuous coating process. In the last chapter (§6), we investigate the effectiveness of GO single layers as molecular blocking layers to protect AgNW electrodes from degradation under current flow.

3 High-Yield Deposition and Continuous, Barrier-Free Langmuir-Blodgett Transfer of Graphene Oxide Single Layers

As discussed in §2.3.2, previous work has focused on dispersing GO sheets at the air-water interface from water miscible solvents (see Table 2.1) which leads to significant loss of materials into the sub-phase water. Moreover, although the traditional LB technique has proven to be a promising method to produce GO single layer films, the size of resulting film is limited by the configuration of commercial LB trough. In this chapter, we introduce a colloidal dispersion strategy to improve the transfer efficiency of single layer GO sheets to the air-water interface by engineering majority water immiscible spreading dispersions. Moreover, we demonstrate that the resulting Langmuir films are not repulsive, as previously suggested, but the sheets are attractive and form uniform and dense domains that grow from the edge of the Langmuir trough inwards. Taking advantage of this effect, we demonstrate a barrier-free densification method which enables rapid growth and deposition of large area films of GO monolayers where we are able to demonstrate a surface coverage of over 800 m^2/g which closely matches the surface area of dispersed GO under infinitely dilute conditions. The effects of GO concentration and lateral sheet size distribution on the transfer efficiency and film morphology are assessed.

3.1 Experimental

3.1.1 Graphite Oxide Synthesis

Graphene oxide (GO) was prepared using the Tour's method.[35] In a typical reaction, 3 g of graphite (Alfa Aesar, -10 mesh, 99.9%) was added into a mixture of 360 mL of H_2SO_4 (Sigma-Aldrich, 95 – 98%), and 40 mL of H_3PO_4 (Sigma-Aldrich, extra pure, 85% solution in water) in a flask and stirred at room temperature. Then, 18 g of $KMnO_4$ (Sigma-Aldrich) was slowly added. The temperature of the mixture was maintained at 40 ºC. After stirring for 16 h, the mixture was cooled down to room temperature. Finally, the mixture was transferred into a large beaker filled with 400 g of ice, followed by the slow addition of 3 mL of 30% H_2O_2 (Sigma-Aldrich). The color of the solution turned from dark brown to golden. The resulting mixture was separated from the residual acids by centrifugation. The pellet was redispersed with 30% HCl (Sigma-Aldrich) and centrifuged again. This process was repeated once more, followed by four washes through centrifugation with ethanol (Fisher Scientific) to remove the HCl. The resulting GO slurry was stored in ethanol.

3.1.2 Graphene Oxide Spreading Suspension

The as-prepared GO dispersion in ethanol was diluted (if necessary) and mixed with 1,2-dichloroethane (DCE) (residue-free, electronic grade, Fisher Scientific, 99.9%) to make a final GO dispersion at the desired concentration with a volume ratio of ethanol/DCE of 1:13. A dilute GO in ethanol dispersion at a concentration of 1.4 mg/mL was prepared from the ethanol stock followed by 5 min of tip ultrasonication. Longer ultrasonication, (10 min) was used to break up the sheets into smaller diameter as discussed later. This ethanol dispersion was then diluted with residue-free DCE into the volume ratio mentioned above, final concentrations of 0.1 mg/mL, 0.05 mg/mL, 0.025 mg/mL, 0.00625 mg/mL and 0.003 mg/mL were used in this work.

The GO in methanol dispersion was prepared via solvent exchange of the GO suspension in ethanol. Typically, the GO dispersion in ethanol was centrifuged at 4000 rpm and the pellet was redispersed with methanol and centrifuged again. This step was repeated twice more. Then, the GO was stored in methanol. A dilute GO in methanol dispersion at a concentration of 1.4 mg/mL was prepared immediately from this methanol stock, followed by 5 min of tip ultrasonication. The final traditional GO spreading dispersion at the concentration of 0.025mg/mL was prepared by diluting this GO in methanol dispersion with water at a volume ratio of 5:1.

3.1.3 Barrier-Free Deposition

A glass trough with Teflon tape wrapped edges and barriers was used to carry out the barrier-free deposition of the large area Langmuir film. The trough was cleaned with DCE and rinsed with deionized water (MilliQ) and then filled with water until the water surface emerged just passed the trough walls. The air-water interface was cleaned using an aspirator. The cleanliness of the trough was verified by using a filter paper Wilhelmy plate and a balance. The water surface tension was measured as 72 ± 0.5 mN/m. Substrates such as mica and clean PET were placed underneath the water prior to the deposition. A spreading suspension of GO was prepared according to the procedures discussed above. The spreading dispersion was dripped onto the air-water interface using a clean glass syringe and Teflon tubing with inner diameter of 159 µm and outer diameter of 312 µm using a syringe pump (KD Scientific, model 230) at a rate of 0.13 mL/min. As each droplet of the suspension contacted the water surface, the solvent spread spontaneously due to the positive spreading coefficient, and then evaporated, leaving the materials floating at the air-water interface. Dripping was continued until the solvent could no longer spread as indicated by the formation of lens of solvent under the dripping position. The resulting film was then deposited onto arbitrary substrates by the horizontal precipitation method which involves slowly draining out the water from the trough, such that the film is lowered onto the substrates placed beneath the sub-phase water. Substrates were air dried prior to collecting them from the trough for further analysis. A schematic of barrier-free deposition as well as horizontal precipitation approach are shown in Figure 3.1.

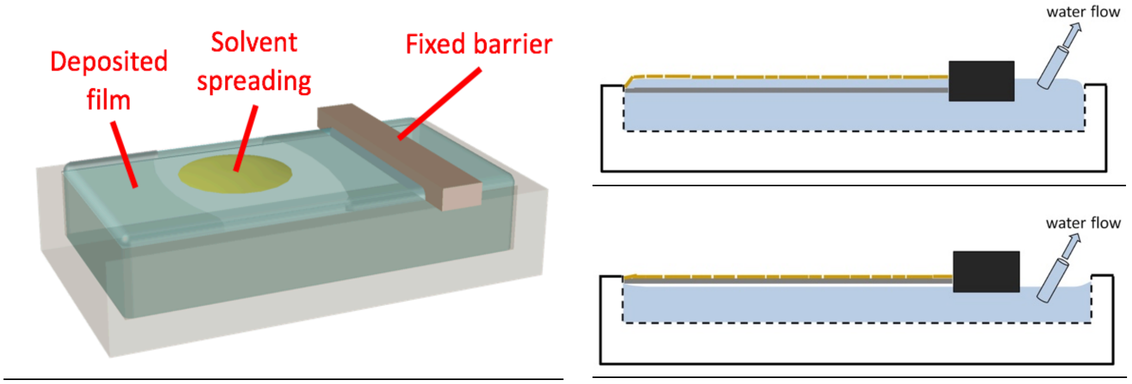

Figure 3.1 Schematic of the barrier-free deposition (left) and horizontal precipitation method (right)

3.1.4 Repetitive Dripping Deposition on Commercial LB Trough with Fixed Barriers

The Teflon trough (NIMA, KN1006) was carefully cleaned by ethanol and then rinsed with MilliQ water. Then 600 mL of MilliQ water at desired pH was prepared using NaOH solution to adjust the water to pH=10 and HCl solution to adjust to pH=4. Approximately 500 mL of MilliQ (or pH adjusted) water was then added into the trough and the cleanness of water surface was examined by monitoring the changes of surface pressure while the barriers of the trough were being closed. The surface was cleaned by a vacuum aspirator until the surface pressure changed by less than 0.02 mN/m. The arrangement of barriers, fixed Brewster angle microscope (BAM) (mode) and dripping position were shown in Figure 3.2, where the barrier on the left was placed 3 cm away from the field of view of the BAM while the other barrier was 14 cm away. The as-prepared GO suspension in DCE/ethanol mixture (v:v = 13:1) was dripped onto the water surface at a speed of 0.13 ml/min. Since the spreading disturbs the position of the interface, the dripping had to be paused each time a BAM video recording/snapshot was taken in order to focus the image. The videos were taken after dripping for 0.5 – 1min depending on the stage of deposition until the solvent could no longer spread as indicated by pooling of the solvent at the deposition site. At this point the water was removed from the trough by vacuum aspiration.

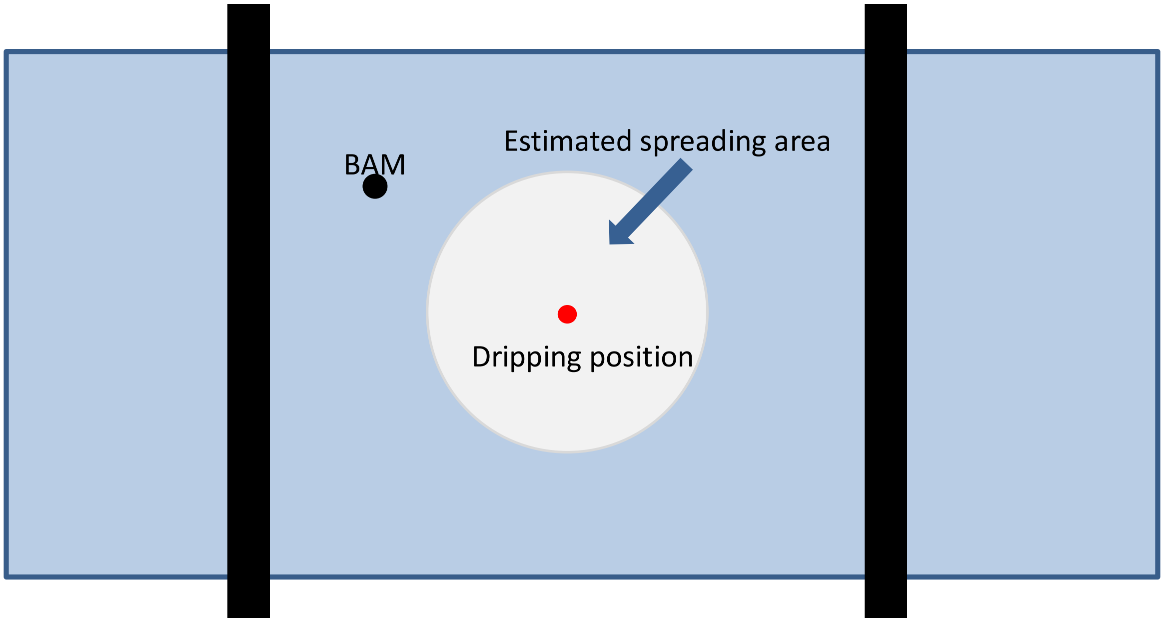

Figure 3.2 Configuration of BAM and dripping position.

3.1.5 Compression-expansion Isotherm experiment on commercial LB trough

The Teflon trough (NIMA, KN1006) was carefully cleaned by ethanol and then rinsed with MilliQ water. Approximately 500 mL of MilliQ water was then added into the trough and the cleanness of water surface was examined by monitoring the changes of surface pressure while the barriers of the trough were being closed. The surface was cleaned by a vacuum aspirator until the surface pressure changed by less than 0.02 mN/m and the barriers were then open to the two sides. 3 mL of as-prepared GO suspension in DCE/ethanol mixture (v:v = 13:1) at the concentration of 0.00625 mg/mL was dripped onto the water surface at a speed of 0.13 mL/min. The interface was stabilized for 30 min. Then the isotherm graph was obtained by closing the barriers at a speed of 15 mm/min to achieve the target surface pressure up to 5 mN/m, and opening the barriers at the same speed. This step was repeated to collect the isotherm data for surface pressure up to 10 and 15 mN/m.

As for the experiment of comparing our spreading solvent with the traditional one (methanol and water mixture), the trough was prepared and cleaned as described in last paragraph. Then, 4 mL of as prepared GO suspensions in methanol/water mixture at the concentration of 0.025 mg/mL was dripped onto the water surface at a speed of 0.13 mL/min. The interface was stabilized for 20 min. Then the isotherm graph was obtained by closing the barriers at a speed of 15 mm/min until it reached the smallest surface area. Typical initial and final surface areas were around 760 and 97 cm^2. The steps were repeated to obtain isotherm data with as prepared GO suspensions in ethanol/DCE mixture. The BAM videos were taken during both isotherm experiments.

3.1.6 Fabrication of rGO Monolayers Coated Ag Nanowire Electrodes

The AgNW/PET samples were prepared through collaboration work with Dr. Goldthorpe's research group. [65] The GO monolayer-coated AgNW/PET samples were prepared by depositing our Langmuir GO film on AgNW/PET samples. The resulting samples were dried in a vacuum oven at 60 ºC for 1 h to remove adsorbed water. A 50 mM solution of $NaBH_4$ (Fisher Scientific) in water (pH adjusted to 10 using NaOH) was heated to 50 ºC.[66] Coated samples were immersed in this solution for 15 min, followed by rinsing with DI water. The resulting chemically reduced films were dried in a vacuum oven at 60 ºC for 1 h.

3.1.7 Film Characterization

Contact mode AFM was carried out on GO films deposited on atomically flat muscovite mica (SPI) substrates using NP-STT10 tips (Bruker) and a Nanoscope MultiMode AFM (Veeco). AFM images were analyzed using Gwyddion software to extract height profiles between the atomically smooth substrate and the GO sheets, and a custom MATLAB code was used to estimate sheet thicknesses from the steps in the height profiles.

A Brewster angle microscope (BAM) from KSV NIMA Techniques was used to enable visualization of GO monolayers at the air-water interface. The imaging resolution limit is ~2μm.

3.1.8 Calculation of Langmuir Specific Surface Area

In order to estimate the transfer efficiency of the sheets to the air-water interface, we define the Langmuir specific surface area (LSSA) which provides the mass specific surface area of GO per trough area covered. The trough area is 17.5 cm × 12.5 cm and the area occupied by the lens of solvent at the end of the deposition is ~15 cm^2. Therefore, the film coverage was ~$17.5\times12.5 - 15 = 204$ cm^2. In order to compare to the specific surface area (SSA) of GO reported in the literature we used $0.0204\times2 = 0.0408$ m^2 as the GO film area since it has two sides. As a result, the LSSA value can be easily calculated by 0.0408 m^2 divided by the mass of floating materials deposited, which is in a unit of gram.

3.1.9 Zeta potential (ζ) Measurement

ζ -potential was measured in various pH buffers using a Malvern Zetasizer Nano ZS90 instrument with a 10 mM NaCl background electrolyte in the GO aqueous dispersion. Acetate buffer was used for pH = 3, 4, 5 and 6. HEPES (4-(2-hydroxyethyl)-1-piperazineethanesulfonic acid) buffer was used for pH = 7 and 8. Bicarbonate buffer was used for pH=10.

3.2 Results and Discussion

3.2.1 Graphene oxide dispersions in water-immiscible spreading solvents

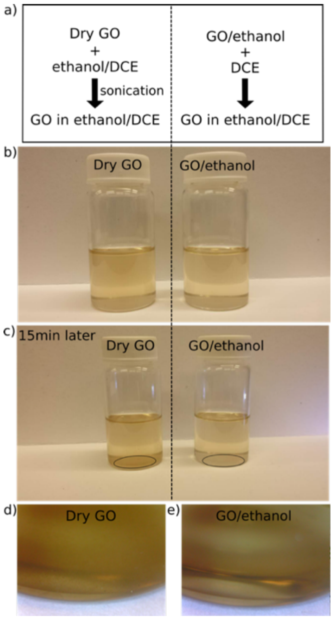

Figure 3.3 Dispersion quality of GO prepared from different processing routes (I): Dispersing dry graphene oxide in ethanol/DCE mixture (a left) and mixing graphene oxide in ethanol dispersion with DCE (a, right). Photos of graphene oxide suspensions in ethanol/DCE mixture right after preparation (b) and 15 min later (c). The zoom-in view at the bottom of the bottles in (c) were shown in (d) and (e). Note that compared to the suspension obtained from ethanol dispersion of graphene oxide, precipitates were observed in the suspension prepared from dry graphene oxide 15 min after preparation.

Figure 3.3 illustrates the dispersion quality of GO after two different processing routes: (1) dispersing dried GO powder in a mixture of ethanol and DCE and (2) mixing GO dispersed in ethanol (without drying) with DCE. After long bath plus tip ultrasonication of mixtures prepared by adding the dry GO powder to the solvents (ethanol/DCE mixture with a volume ratio of 1:13 ethanol to DCE), the material appears dispersed, as shown in Figure 3.3b. However, aggregates were observed at the bottom of the vial approximately 15 min after sonication (Figure 3.3c,d). Preparing Langmuir films from this suspension, which will be introduced in a later section (§3.2.3), leads to extensive wrinkling and overlaps between sheets as observed after transfer to substrates by AFM as shown in Figure 3.4. On the other hand, GO could be well-dispersed in ethanol, especially if the dispersion was not dried after the washing steps of Tour's modified Hummer's method. Mixing a small amount of this stock solution of pre-dispersed GO with DCE (volume ratio of 1:13 ethanol to DCE) led to a dispersion which was stable for at least several hours which was sufficient time to deposit LB films. After several hours, visible aggregates began to precipitate at the bottom of the vial and could not be effectively re-dispersed by ultrasonication. Thus ethanol dispersions and DCE were mixed just prior to each deposition.

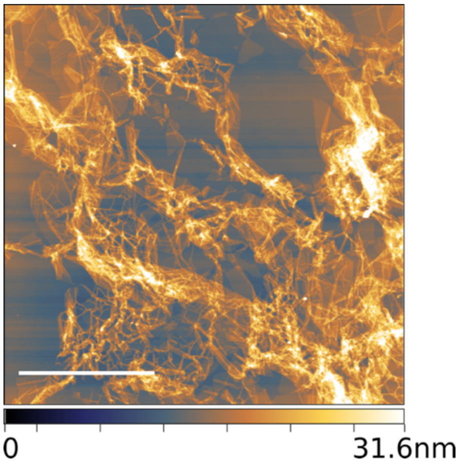

Figure 3.4 Dispersion quality of GO prepared from different processing routes (II): AFM image of GO film created by GO dispersion in DCE/ethanol (volume ratio of 13:1) prepared by adding dry GO powder to DCE/ethanol mixture followed by 10 min bath sonication and 5 min tip sonication. The scale bar is 5 µm.

3.2.2 Traditional LB films with improved spreading solvent

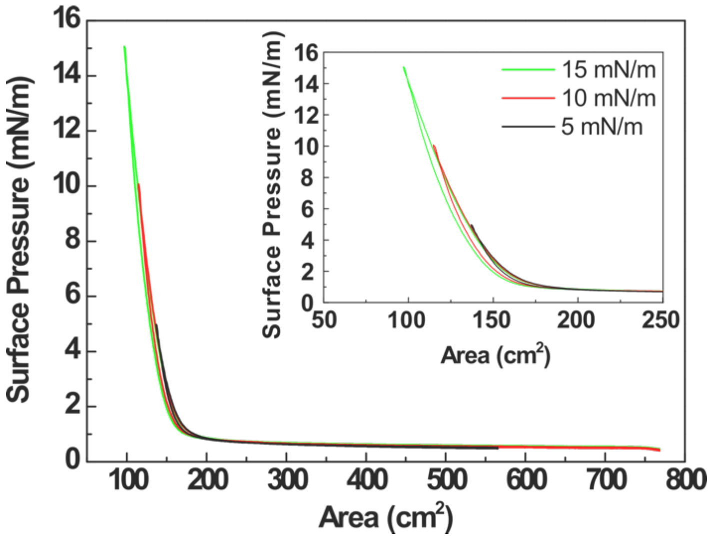

Figure 3.5 Compression-expansion isotherm experiment of LB GO film from the DCE-based spreading solvent under dilute conditions: *Π*-A isotherms of three sequential compression-expansion cycles when surface pressure targeted up to 5 mN/m (black curve), 10 mN/m (red curve) and 15 mN/m (green curve), respectively. Inset shows magnified view of the last stage of three cycles. Note that no significant shift is observed in either of three compression-expansion loops, suggesting that GO monolayers are repulsive and charge stabilized at the air-water interface.

Figure 3.5 shows a typical surface pressure-area (π-A) isotherm recorded using a commercial LB trough after spreading a dilute (0.00625 mg GO/mL) dispersion from the majority DCE solvent. After 20 min of stabilization, the floating GO films were densified by mechanical barriers and then expanded. Up to π = 15 mN/m, no significant hysteresis between compression and expansion was observed. This observation is in line with what has been shown previously for GO deposited using methanol/water as the spreading solvent.[1] This reversibility supports the view that floating GO are repulsive and charge stabilized at the air-water interface by the electric double-layer repulsion generated by charged functional groups such as dissociated phenolic hydroxyls and carboxylic acids which exist mainly at the edges of the floating GO sheets.

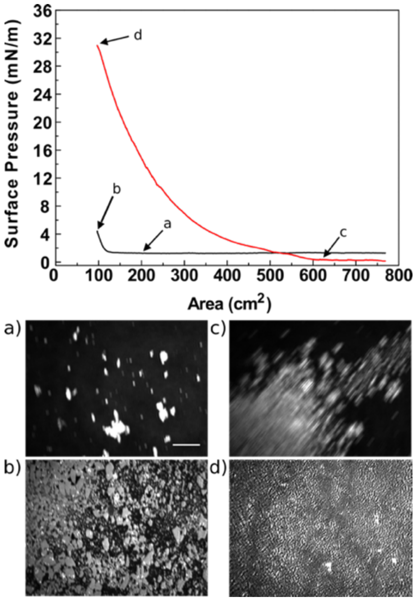

Figure 3.6 High-yield transfer of GO sheets by using the DCE/ethanol-based spreading solvent instead of methanol/water-based one. Compression isotherm obtained by transferring same amount of GO sheets onto the air-water interface via two different spreading solvents: methanol/water (volume ratio of 5:1) (black curve) and ethanol/DCE (volume ratio of 1:13) (red curve). Corresponding BAM video snapshots (a-d) of film morphologies over the process were labeled on the curves. Scale bar in (a), which is effective for all the other BAM images (c-d), is 100 μm.

The significant improvement in transfer efficiency between the DCE/ethanol-based and methanol/water-based spreading solvents is shown in Figure 3.6. Compression isotherms and *in situ* Brewster angle microscope (BAM) images are shown for experiments where the same mass and concentration (0.025 mg/mL) of GO was deposited from each spreading solvent system. The methanol/water case shows a shifted baseline from zero surface pressure due to the mixing of methanol and water that causes a decrease in the surface tension of water. In this case, compressing the film to an area of ~200 cm^2 increases the density of what are observed (Fig. 3.6a) to be discretely floating sheets and some clusters. Further compression to nearly 100 cm^2 (the limit of the trough) resulted in a denser but incomplete monolayer (Fig. 3.6b). On the other hand, for the DCE case, at 625 cm^2, larger mobile clusters are observed (Fig. 3.6c) while at nearly 100 cm^2, the surface pressure reached 31 mN/m and BAM imaging reveals a fully dense film (at least to the resolution of the BAM, ~1 μm) with some brighter contrast regions which likely correspond to occasional wrinkles and overlaps between the sheets (Fig. 3.6d). A comparison between these two cases indicates three important differences: (i) the transfer efficiency using DCE as a spreading solvent is about five-fold higher than the methanol/water case (compare point b and d); (ii) Large clusters of GO are observed in the DCE case compared to the isolated sheets in the methanol/water case; (iii) The sheets deposited from methanol/water appear much larger (on average) than those deposited from ethanol/DCE. This confirms the size-selection observed by others [27] using methanol/water system and suggests that our new spreading solvent may not exhibit any size selection. This hypothesis will be investigated further in the next section.

3.2.3 Barrier-free densification of Langmuir films

Given the significant clustering and 2D island formation observed with the DCE-based spreading solvent, we decided to study the dynamic deposition process on a more macroscopic level using video to capture the spreading process over the entire trough. In this case, a clean glass dish with Teflon coated walls was used to provide more suitable contrast between the film and bath than the commercial LB trough. Snapshots of video taken after repetitively dripping a 0.025 mg/mL dispersion at the air-water interface are shown in Figure 3.7a-c. The video was paused at the point when a drop of the spreading dispersion was deployed and had spread to its maximum area. A boundary between the evaporating solvent and what was suspected to be the adjacent film covered interface is clearly visible. As more drops of dispersion are added to the trough, the spreading area is observed to shrink which suggests that the observed boundary moves inward as the film grows. Continuing this process leads to a further decrease of the spreading area until the solvent could no longer spread and forms a liquid lens that sits at the interface for several seconds before evaporating. To confirm this boundary is indeed between the spreading solvent and a growing film, we also carried out the same experiment using the commercial LB trough while observing film deposition by BAM (Fig. 3.7d-f). Since the BAM position is fixed, we could only observe the boundary ~5 cm from the dripping position. With each drop, material was observed to move rapidly past this position but pausing to take a snapshot indicated that the water surface was free of any floating material during the early stages of deposition. After 0.042 mg of GO was deposited, there was an abrupt transition from a clean interface to a densely tiled film that grew across the field of view with each additional drop. Pausing the dripping to capture a focused image indicated that the film remained densely tiled but convection (likely introduced by air-currents above the trough) could induce the sheets at the boundary between the clean water and dense film to move and tumble (in 2D) rapidly past one another while seeming to maintain some attraction to the growing front. Adding more GO to the trough caused the film to move past the field of view of the BAM. This uniformly dense film remained solid if the barriers were paused to take a snapshot as shown in Fig. 3.7f.

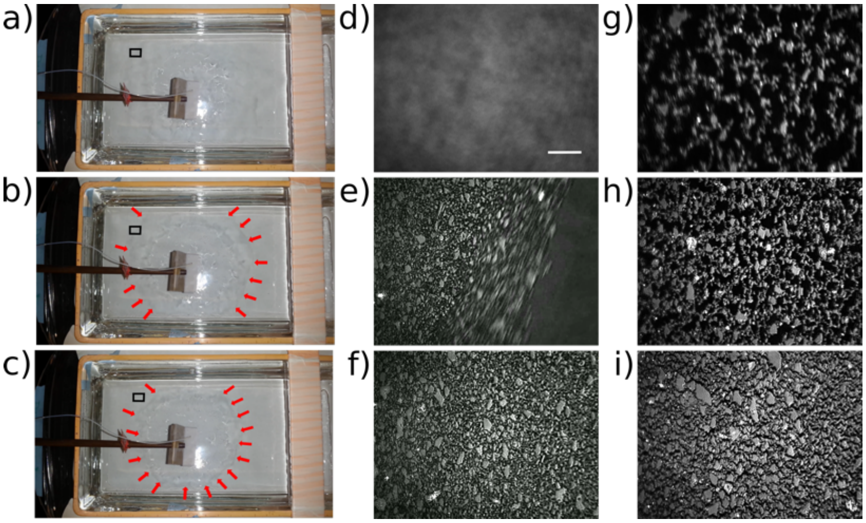

Figure 3.7 Macroscopic and microscopic observations of GO film formation via repetitive dripping process: snapshots of videos recorded through the process (a, b, c). The interface between growing GO film and solvent spreading is labelled by red arrows in (b) and (c). Note that at the early stage (a) of the deposition, the interface is unclear to be captured. Snapshots of *in situ* BAM videos taken at the interface between the spreading solvent and 'growing' film using a typical concentration of GO dispersions at 0.025 mg/mL (d, e, f) and 0.00625 mg/mL (g, h, i) respectively. The position where *in situ* BAM were set is labeled as black squares in a, b and c. Scale bar in (d), which is effective for all the other BAM images (e-i), is 100 µm.

On the other hand, if a lower concentration dispersion of GO in DCE/ethanol is used, we observe a different phenomenon. Figure 3.7g-i show snapshots from the BAM when a 0.00625 mg/mL dispersion is continuously dripped onto the trough. After depositing 0.024 mg (Figure 3.7g) a low density network is observed of what appears to be a mixture of isolated sheets and small clusters of 5-10 sheets aggregated in a branched morphology. As deposition is continued, this network densifies and eventually yields what appears to be an equivalent packing density as with the more concentrated case although it happens at a relatively later time during the deposition.

To determine if the packing density changes as a function of position in the trough (since the BAM is fixed in position) and to confirm that our process yields single layers of graphene oxide, we coated mica pieces at various positions within the trough and coated them by the horizontal precipitation method (which simply lowers the film onto the substrates placed beneath the surface prior to deposition). In Figure 3.8, we show representative AFM images from various positions (indicated in the figure) and the two different deposition concentrations. Some wrinkles and overlaps at the edges of sheets were observed in high concentration condition. As shown in Figure 3.9(a,b) the 0.00625 and 0.025 mg/mL depositions both yield a densely tiled layer of sheets which are 0.7-1 nm in thickness (Figure 3.10), as is known to be the case for single layers of GO, with some wrinkles and occasional overlaps between adjacent sheets.

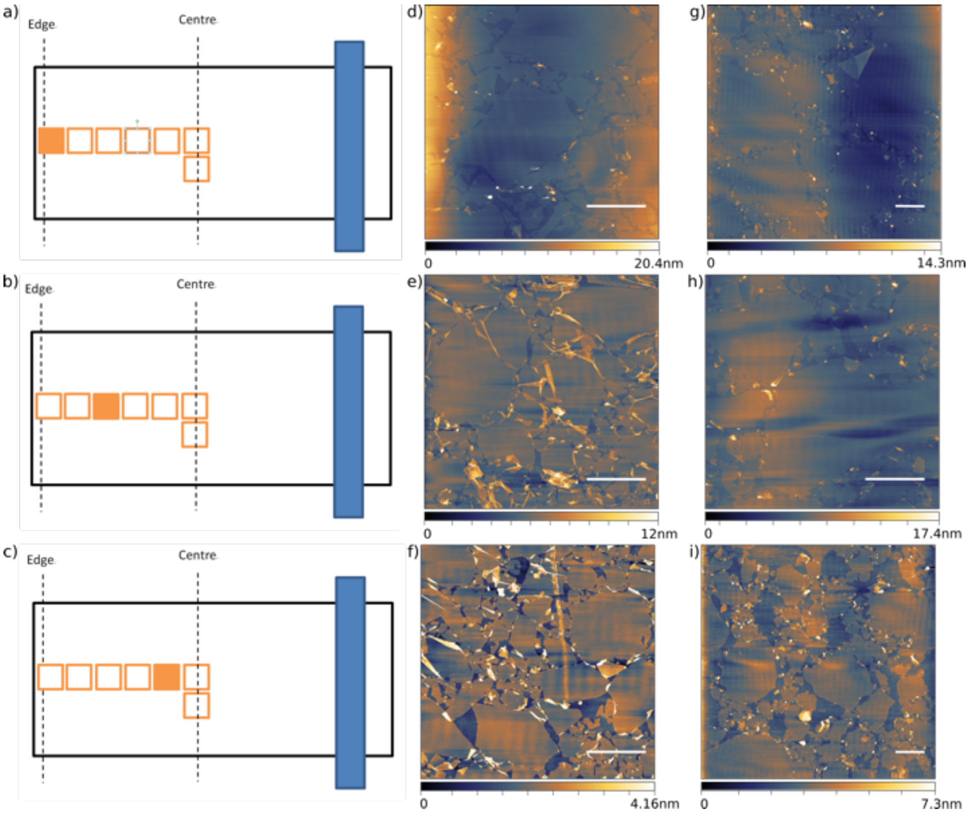

Figure 3.8 Morphology of GO film by barrier-free deposition: AFM images of as-prepared GO film at concentration of 0.025 mg/mL (d-f) and 0.00625 mg/mL (g-i). Schematics illustration of the corresponding mica substrates positions in the trough are shown in a, b and c. The scale bar in d-f and g-i is 5 µm.

This wrinkling becomes much more pronounced when higher concentrations (0.1 mg/mL and above) are used as shown in Figure 3.9c. In order to further verify uniform coverage, these films were also chemically reduced which tinted films deposited on transparent substrates such as polyethylene terephthalate (PET) as shown in Figure 3.9(d,e). While films with concentration at or below 0.025 mg/mL were visibly uniform, the wrinkling observed in the higher concentration cases translated to a non-uniform and textured film where wrinkled and overlapping regions appeared darker.

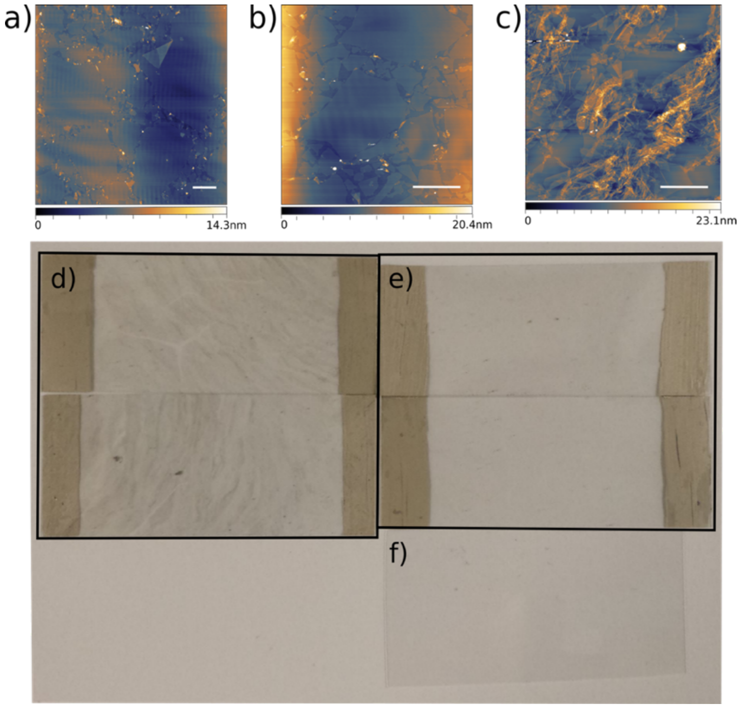

Figure 3.9 Concentration effect on GO film morphology produced by barrier-free deposition: packing density of GO films verified by AFM images at three different concentrations: 0.00625 mg/mL (a), 0.025 mg/mL (b) and 0.1 mg/mL (c). AgNW/PET substrates coated with as-prepared GO film after chemical reduction from different concentration: 0.025 mg/mL (d) and 0.1 mg/mL (e). Plain PET (f). Note that uniform GO monolayer film were obtained with concentration at or below 0.025 mg/mL (a, b and e) while wrinkles and overlaps were observed between sheets when higher concentration was used (c and d). The scale bar in a, b and c is 5 µm.

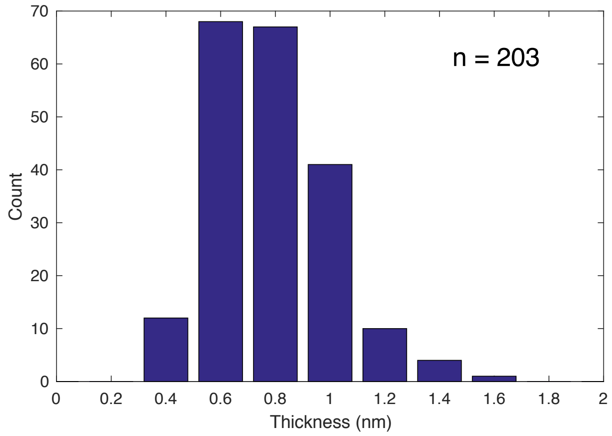

Figure 3.10 Graphene oxide sheet thickness analysis: histogram of graphene oxide sheet thickness estimated from AFM imaging

After verifying the film uniformity, it became possible to more accurately estimate the film transfer efficiency in terms of the Langmuir specific surface area (LSSA) which estimates the area of GO (both sides) per g of GO deposited. Figure 3.11, shows estimates made using the measured trough area after forming a densely tiled film and dividing this area by the known mass of GO deposited. At concentrations between 0.003 and 0.025 mg/mL we reproducibly observe LSSAs of 700 - 800 m^2/g. There could be a small error, ~5%, in the estimation as the trough area was not completely covered by GO film. Even if we count the 5% error in the estimated values, it's still quite close to the highest literature SSA value estimated for GO, by using the method of methylene blue titration of stable single layer GO dispersions, which is 889 m^2/g.[67] Therefore, we conclude that by using our repetitive dripping deposition, we achieve a high efficiency, nearly 100%, in terms of transferring GO single sheets onto the air-water interface which assembled into large area monolayer films. However, the LSSA values we estimate begin to drop at higher concentrations where we observe significant overlapping between sheets via AFM as shown in Figure 3.9c.

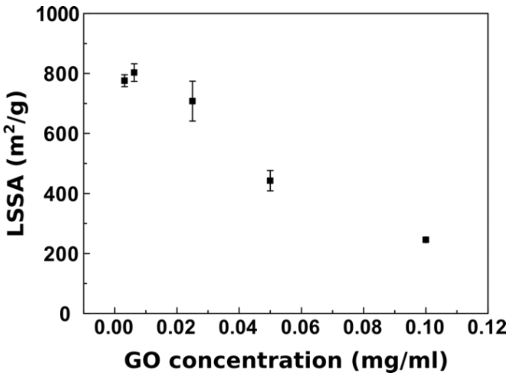

Figure 3.11 Concentration effect on estimated LSSA: change of estimated LSSA of the prepared GO films as a function of the concentration of GO dispersion in ethanol/DCE (1:13) mixture.

As shown in Figure 3.12 by using longer time ultrasonication (10 min vs. 5 min), the lateral sheet size is significantly reduced with the majority of sheets exhibiting diameters below 1 μm. However, we observed 800 ± 30 m^2/g from large sheet size suspension and 700 ± 80 m^2/g from small sheets size suspension in the LSSA obtained after our barrier-free deposition process. This indicates that there is no size effect with our deposition process. In addition, this challenges the view that only large sheets float [27] which is an effect that has been observed by various authors which has made it impossible to carry out studies of sheet size effects by LB deposition in various applications.

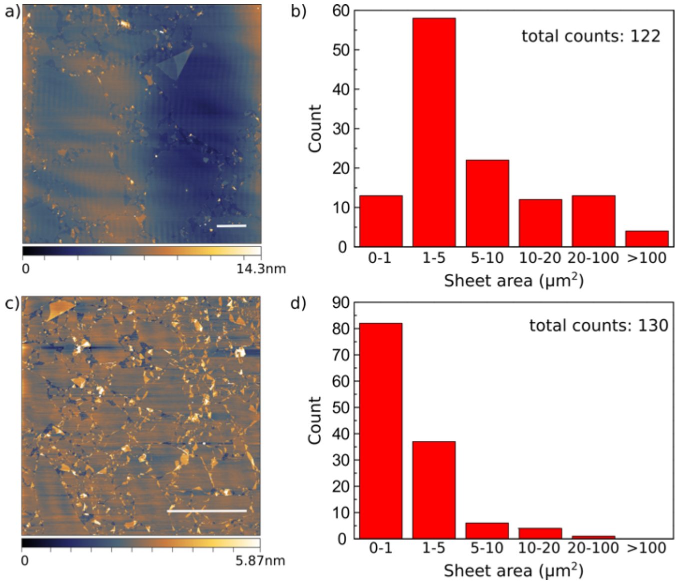

Figure 3.12 Study of size-effect in barrier-free deposition: AFM images of as-prepared film with GO dispersions composed of large diameter sheets (a) and smaller diameter sheets (c). And corresponding histogram of sheet area distribution of big-sheets GO dispersion (b) and small-sheets GO dispersion (d) with insets showing the total number of analyzed sheets in each case. The scale bars in a and b are both 5 μm.

3.2.4 pH effect – study of the aggregation mechanism

In order to better understand the behavior of GO sheets at the water surface during our deposition, in this section, we used the pH value of the sub-phase water to investigate the interaction between sheets floating at the air-water interface. GO produced by chemical oxidation of graphite usually consists of hydroxyl and epoxide groups mainly on the basal plane and phenolic hydroxyls and carboxylic acid groups at the edges.[68–71] When two GO sheets approach each other at the water surface, according to Derjaguin-Landau-Verwey-Overbeek (DLVO) theory, the interaction between the two sheets is determined by the sum of two potentials: van der Waals attractions and electrostatic repulsion. As the degree of ionization on the sheets can be tuned by pH values of sub-phase water, changing the pH of the sub-phase water can be used to manipulate the charge density.[72] This, as a result, can change the electrostatic repulsion force that might be responsible for the edge-to-edge aggregation observed in our studies. The surface charge density can be characterized by measuring the ζ-potential. As shown in Figure 3.13, since less surface functional groups are deprotonated in lower pH, the ζ-potential becomes less negative as the value of pH decreases.

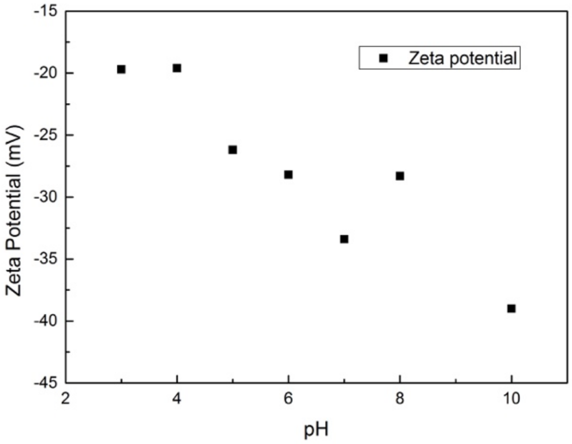

Figure 3.13 Plot of pH-dependent ζ-potential measurement

Thus to determine how the aggregation behavior is effected by trough pH (and possibly GO charge density), depositions from GO dispersions at 0.025 mg/mL were monitored by *in situ* BAM. Snapshots of BAM video taken different time periods in different initial trough pH conditions (pH = 4, pH = 7, and pH = 10) are shown in Figure 3.14. Due to dissolution of carbon dioxide into the water, the pH = 7 case and pH = 10 case decreased to about 6 and 8, respectively over the deposition. In the case of pH = 4, at the early stage of the deposition when only 0.003 mg GO were transferred onto the water surface, we observed large island-like aggregates of close-packed GO sheets moving rapidly on the water (Figure 3.14a). In contrast, when basic sub-phase water was used, well dispersed GO sheets were observed on the water surface (Figure 3.14g), after even more GO was deposited (0.013 mg) via repetitive dripping process. In the case of pH = 7, we observed a large densely-packed island when 0.042 mg of GO was deposited. However, when the dripping was paused for recording BAM videos, the sheets were quite mobile and could be observed to tumble passed one another within the aggregate likely due to the convection of the drying solvent or air currents flowing past the trough (Figure 3.14d). As more materials are added, in all cases, the film is densified throughout the repetitive dripping process regardless the sub-phase pH value, as shown in Figure 3.14(b-c), (e-f), (h-i) respectively. However, there are some qualitative changes in the film packing density which can be observed once the deposition is complete. It appears that the resulting film in the pH = 4 and pH = 10 cases have more pinhole defects while no defects can be observed (within the resolution of the BAM) for the initial pH of 7 case. We hypothesized that this film densification phenomenon could be related to the spreading pressure from solvent which is a crucial constant parameter in all deposition cases. This will be fully discussed in next chapter.

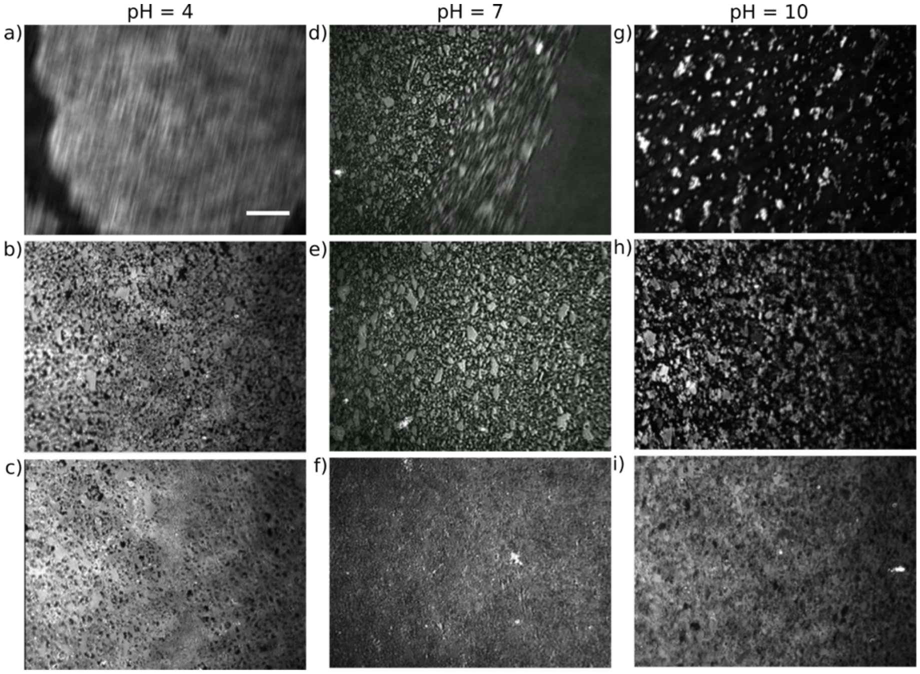

Figure 3.14 Microscopic observations by *in situ* BAM of GO film formation via repetitive dripping process over subphase water at various pH: pH=4 (a-c), PH=7 (d-f), pH=10 (g-i) The scale bar in a is 100 μm and is valid for all other images.

All of these observations suggest that the aggregation mechanism we observe under the higher concentration deposition does depend on bath pH, likely due to the change in the ζ-potential of the sheets floating at the air-water interface. At low pH, the ζ-potential is low and edge-to-edge aggregation appears strong. The more prevalent pinholes in the final film suggest that this stronger attraction makes the sheets less mobile in the aggregate and cannot rearrange as easily to find the most effective packing configuration. At pH = 10 the sheets are more repulsive during the entire deposition process. At the intermediate pH, the sheets are attractive but there appears to be some space (~microns) surrounding each sheet which provides some mobility to the sheets which allows them to rearrange and pack the most effectively. We have attempted to calculate the net attractive/repulsive potentials based on DLVO theory. If the cross-section of each sheet is considered as a flat plate geometry with a cross-sectional area of 1 nm x 1 μm (the thickness times the diameter) is considered we calculate attractive and repulsive potentials which are ~10^{-7} kT. This suggests that van der Waals forces and electrostatic repulsion should not play a role in the aggregation at all. The exact explanation for the observed aggregation phenomena can thus not be explained by DLVO theory alone and will be left of future work. Silverberg *et al.* also observed similar aggregation phenomena of partially reduced GO sheets at the air-water interface. They suggested that the clustering is due to long range attractive forces rather than DVLO interactions.[26]

3.3 Conclusions

In this chapter, by replacing typical spreading solvent with a non-aqueous solvent mixture (ethanol/DCE), we obtained high-yield transfer of GO single sheets onto the air-water interface. We also demonstrated a barrier-free densification process for producing large area Langmuir films of GO which allows us to measure the Langmuir specific surface areas of GO film as high as 800 m^2/g. Moreover, while others have observed that small sheets sink while large sheets float [27], we demonstrate that sheet size has no significant impact on the transfer efficiency and the loss of small sheets in the sub-phase must be related to the miscibility of the spreading solvent with water. By using BAM to enable the visualization of behavior of GO sheets at the interface, we observed the formation of edge-to-edge aggregation of densely-packed GO sheets in high concentration case while the sheets form branches and networks under more dilute conditions. Furthermore, we investigated the pH effect on the aggregation phenomena in the high concentration case. At the early stage of the deposition, compared to the basic condition, where the sheets were well-dispersed on the surface, the formation of densely packed islands were obtained over acidic subphase. We also attempted to calculate the van der Waals attractions and electrostatic repulsion and suggested that this aggregation is a non-DLVO interaction.

4 Film Densification Mechanism

In this chapter, we attempt to determine the underlying mechanism behind the film growth phenomena during the repetitive dispersion spreading process. In §3.2.3, we discussed the observation of edge-to-edge aggregation and film densification under the *in situ* BAM during the deposition process. Regardless of concentration and pH changes, we always observed the film densified through the repetitive dripping process. Thus, we hypothesized that the lateral pressure from spreading solvent could be the driving force for film aggregation and densification. In order to determine whether or not this is the case, we built a custom Langmuir-Adam balance to measure the dynamic spreading force which acts on the film as it grows.

When liquid 1 is placed on liquid 2, the spreading of upper liquid (1) on liquid 2 happens if the spreading coefficient $S = \gamma_{2/air} - \gamma_{12} - \gamma_{1/air}$ is positive, where $\gamma_{2/air}$ and $\gamma_{1/air}$ is the surface tension of liquid 2 and liquid 1, respectively, and γ_{12} represents the interfacial tension between the two liquids. When spreading occurs, the initial spreading movement is mainly due to gravity. When the liquid film can no longer be thinned by gravity, the spreading is dominated by the gradient of interfacial tensions (known as the Marangoni effect), as shown in Figure 2.5. While the sign of S indicates whether or not spreading can occur, its magnitude should be related to the driving force for spreading. The dynamics of spreading are highly correlated to the viscosity of the two liquids as well as the evaporation rate of the upper liquid. In the case of solvent spreading coupled with evaporation, which usually the case for the LB technique, where a volatile organic solvent is usually used to transfer material to the interface without leaving residue behind, evaporation of this solvent has been shown to reduce the spreading force due to the formation of a thermal convective layer induced by the evaporation process.[59]

In conventional LB deposition of lipids and other small molecules, spreading is not typically considered since all material can be injected at once as only ~100 μL of volume is required since these material can be dissolved in the spreading solvent at much higher concentration than 2D nanomaterials (1 mg/mL vs. ~0.01 mg/mL). In order to determine whether or not spreading plays a role in the film aggregation and densification we observed in our process, we sought out to directly measure the force acting at the spreading front. One of the first devices used to measure changes in surface pressure at the air-water interface was developed by Langmuir and Adam, and is now called a Langmuir-Adam balance. This instrument operates through the use of a lightweight, rigid, floating boundary which is connected to a torsion balance. As an insoluble film spreads onto the air-water interface, the outward pressure acting on the float can be determined by the float's small deflection under the force. Since the surface pressure can also be interpreted as a decrease in the surface tension at the air-water interface, methods to measure surface tension such as the Wilhelmy plate and deNuoy ring methods have become more common than the Langmuir-Adam balance. However, these approaches require a quiescent water surface and the assumption of zero contact angle. Since our approach requires continuous dripping, these methods are not able to measure dynamic changes during spreading, especially when a solvent other than water contacts the plate/ring for which the contact angle changes. To by-pass these challenges, we decided to revive the older version of Langmuir-Adam balance for this work as it is not sensitive to contact angle and can potentially yield dynamic information.

In this Chapter we first discuss the design of a Langmuir-Adam balance and its validation using stearic acid which has a well-known equilibrium surface pressure. Then, we use this balance to measure the spreading pressure changes of the pure spreading solvent used in our GO deposition as a function of distance between the dripping position and the barrier. Lastly, we discuss our hypothesis of the film densification mechanism by combining BAM observations and spreading pressure measurements obtained during repetitive dripping process of GO sheets.

4.1 Experimental

4.1.1 Langmuir-Adam balance setup

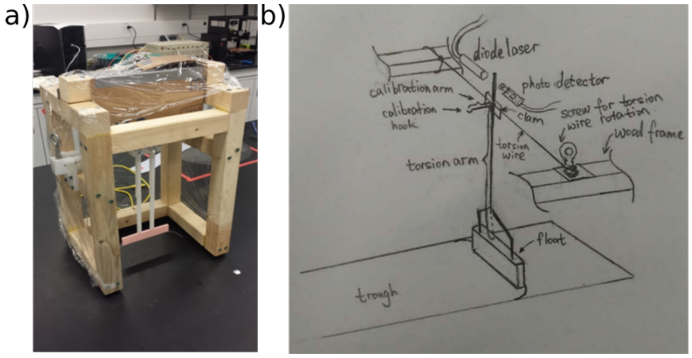

Figure 4.1 Custom-made Langmuir-Adam balance: (a) a photo of the instrument; (b) Schematic illustration of the design of the balance.

A photo of our custom Langmuir-Adam balance as well as a detailed schematic illustration of the functioning parts are shown in Figure 4.1. The components of the balance were mounted on a wood frame. Adjustable feet were added to each leg so that the balance could be easily levelled. A stainless steel torsion wire is fixed on one horizontal arm and then wired and tightened around a big screw on the other parallel one. A torsion arm is attached to the torsion wire by a small clamp. The end of the torsion arm is connected to the floating barrier dividing the trough area into two. The barrier, which was coated with Teflon tape was designed to be 11 cm long, 2 cm wide and 5 mm thick, leaving 5 mm gaps at each end. In order to prevent materials from escaping from film forming side to the clean side, two 1.5 cm long Teflon threads were attached to the two ends of the barrier. A calibration arm was extended out from the clamp, which is perpendicular to the torsion arm, with a hook at the end. The torsion arm is extended out as a 2 cm long stick above the clamp, which is located between a laser diode and a photo detector. The diode and the detector are wired into a circuit on an Arduino UNO shield board. Initially, most of the light is blocked by the stick when the barrier is sitting straight at the clean air-water interface. When the surface tension on the two sides of the barrier are different or a net force acts on the barrier (for example, resulting from solvent spreading) the torsion arm moves and more light hits the photodetector. The change in light intensity results in a change in the output voltage on photo detector which is recorded by computer via the microcontroller on the Arduino UNO board. The communication series between the terminal (computer) and the microcontroller is set to be 9600 so that voltage values will be recorded every 0.01 second. The sensitivity and accuracy of the balance will be discussed in *Results and Discussions* section. Before each measurement, the baseline voltage reading at the initial position was adjusted to a value around 515 – 520 mV by shifting the position of torsion wire, as a consequence the blocking stick. Note that the detector will not be sensitive enough if the value of baseline is below this range. The calibration curve is obtained before each spreading pressure measurement. It is processed by recording the corresponding voltage values when a set of weights with different known mass are hung up on the calibration hook. As for a certain weight with a mass of m (in g), one can calculate the corresponding force exerted along the floating barrier as:

$$F = m \times g \times x / \, (y + d),$$

where g is gravitational constant, x and y represent the length of the calibration arm and torsion arm below the clamp, which are 2.8 cm and 22.3 cm respectively, and d is the width of the float. Therefore, each mass value can be converted into a spreading pressure value acting along the barrier by dividing F by L, where L is the effective length of floating barrier, which is given by the real floating barrier length plus the width of the gaps at one end of the barrier.[63] In our case, L = 11 + 1/2 (0.5+0.5) = 11.5 cm. Thus, the calibration curve can be attained by plotting each spreading pressure value vs. the corresponding voltages. Note that calibration is processed before each measurement in order to ensure the accuracy of the measurement.

4.1.2 Spreading pressure measurement with stearic acid

The trough was again first cleaned with DCE and rinsed with MilliQ water. It was then placed under the levelled Langmuir-Adam balance and the floating barrier was placed 6 cm away from right edge. A large glass was placed in the trough as it was in a regular deposition. The trough was then filled with MilliQ water. After baseline adjustment and calibration (as discussed above), a droplet of 0.015 M stearic acid in chloroform, prepared freshly before the experiment, was placed on the water surface and the voltage changes was recorded. Typically, one additional droplet was added to ensure a monolayer film covered the entire air-water interface. This measurement was repeated another two times. Note that between each measurement, the trough and floating barrier were cleaned to minimize contamination.

4.1.3 Spreading pressure measurements with GO suspension

The trough and balance were prepared through the same steps as discussed in the last section. Freshly prepared GO dispersion in the DCE/ethanol mixture at a concentration of 0.025 mg GO/mL was added onto the water surface area (*A*) in the same way as was carried out in the regular barrier-free deposition. The photodetector voltage was recorded and plotted as a function of time and curves were processed using a custom MATLAB code. The steps were repeated for the more dilute concentration (0.00625 mg/mL).

4.1.4 Data processing method

A typical data processing result is shown in Figure 4.2. A custom Matlab function was applied on the raw data to pick out all the maximums, labelled as green circles, as well as the minimums which are labelled as red circles.

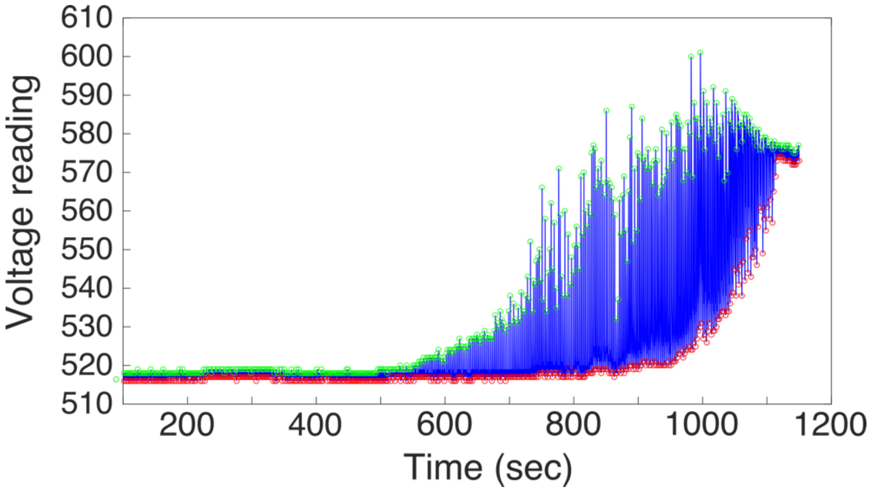

Figure 4.2 Data analysis of spreading pressure measurements: All the maximums (green circles) and minimums (red circles) are picked out after data processing

4.1.5 Compression-expansion Isotherm experiment on commercial LB trough

The Teflon trough (NIMA, KN1006) was carefully cleaned by ethanol and then rinsed with MilliQ water. Approximately 500 mL of MilliQ water was then added into the trough and the cleanness of water surface was examined by monitoring the changes of surface pressure while the barriers of the trough were being closed. The surface was cleaned by a vacuum aspirator until the surface pressure changed by less than 0.02 mN/m and the barriers were then open to the two sides. 1.8 mL of as-prepared GO suspension in DCE/ethanol mixture (v:v = 13:1) at the concentration of 0.025mg/mL was dripped onto the water surface at a speed of 0.13 mL/min. The interface was stabilized for 30 min. Then the isotherm graph was obtained by closing the barriers at a speed of 15 mm/min till reaching the smallest surface area and then opening at the same speed to the initial positions. Typical initial and final surface areas were around 500 and 97 cm^2.

4.2 Results and Discussion

4.2.1 Langmuir-Adam balance calibration and validation

A typical calibration curve is shown in Figure 4.3. When the barrier moves away from the baseline at a small angle, the light intensity change is unable to be precisely detected by the light sensor resulting in a low sensitivity at the beginning of the calibration. Therefore, unfortunately, this instrument is unable to accurately measure the spreading pressure below 2 mN/m.

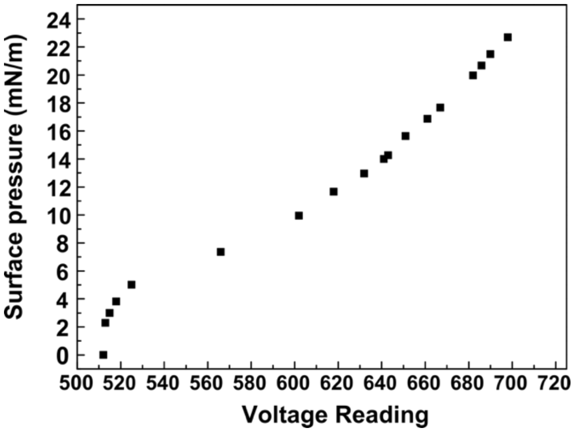

Figure 4.3 Typical calibration curve

We used stearic acid as the insoluble film material to validate the accuracy of our custom Langmuir-Adam balance. A typically measurement result of spreading a droplet of 0.015 M stearic acid in chloroform at the water surface is plotted as voltage vs. time and shown in Figure 4.4. When the droplet is placed on the surface, it spreads out into a transparent thin film, potentially a monolayer film, with the excess remaining as a lens. A sharp increase in output voltage was observe followed by an immediate drop which likely resulted from the initial spreading of the chloroform followed by evaporation. The pressure then maintained a constant value where the stearic acid yielded a stable, equilibrium surface pressure. A second drop was then placed on the water surface, however, it was unable to spread and the voltage remained at the same value. By converting the obtained voltage to the corresponding spreading pressure using the calibration curve, the equilibrium surface pressure of stearic acid was found to be 18.3 mN/m. The measurement was repeat another two times with adjustments to the torsion wire and with new calibration curves processed each time to give us an estimate of the error in our system. The three independent repeats yielded $18 \pm 0.5 \text{ mN/m}$. The literature value of equilibrium surface pressure of stearic acid is 18 mN/m.[73] These results gave us confidence that our Langmuir-Adam balance was capable of measuring equilibrium surface pressures of Langmuir films with both high accuracy and reproducibility. The stearic acid film was found to be stable for several minutes before it started to leak to the other side of the floating barrier which resulted in decrease in surface pressure with time as the pressure equalized on both sides of the trough. This is difficult to avoid as the Teflon thread and the glass wall do not make a stable seal, especially to small molecules. We expect this not to be a significant problem with our GO films since the sheet size is generally ~1-10 μm and the volatile solvent used evaporates within seconds. We also measured the surface pressure of oleic acid, which is also known to act as a piston oil (a liquid capable of maintaining a constant surface pressure).[63,74] However, it could not be used for the validation since the surface pressures (~30 mN/m) were beyond the measurement range of our instrument. Attempts with this oil caused deflection of our sensor beyond the range of good sensitivity.

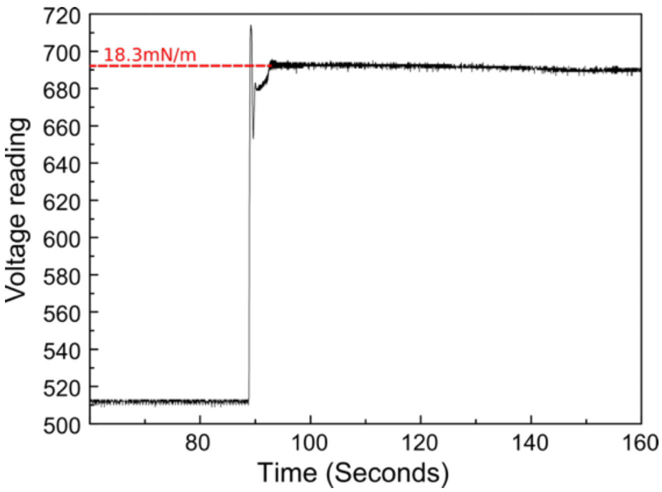

Figure 4.4 Validation of our custom-made Langmuir-Adam balance: Voltage changes as the function of time after one drop of stearic acid in chloroform spreads at the air-water interface and achieves equilibrium. The second drop is placed 30s after the first one. The measured equilibrium surface pressure of stearic acid in this typical experiment is 18.3 mN/m, as labelled, according to the calibration curve.

4.2.2 Dynamic measurements and volatile solvent spreading

In the past, most studies have focused Langmuir film studies on insoluble fatty acids deposited by a single syringe injection of a solution containing these acids onto the air-water interface. Unlike the stearic acid, discussed above, the volatile, water-immiscible organic solvents of interest to our study usually spread rapidly at the air-water interface but also start to evaporate before achieving an equilibrium surface pressure. The surface waves induced by deploying the droplet at the air-water interface as well as the rapid spreading and convection induced by evaporation cause significant movement of the interface which makes it impossible to measure the surface tension using conventional approaches such as the Wilhelmy plate or de Nouy ring. On the other hand, our custom Langmuir-Adam balance reads the force in the horizontal direction and is capable of reading the deflection signal every 0.01 s. A typical spreading pressure measurement result when one droplet is placed on the water surface at an effective distance from measuring float is shown in Figure 4.5. A force is detected over ~0.5 s reaching a maximum before the solvent evaporates.

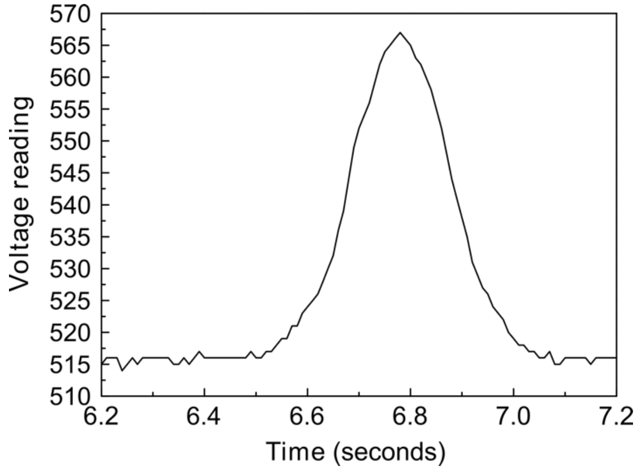

Figure 4.5 Spreading pressure measurement of spreading one droplet of the pure solvent. The dripping position is 3.5 cm away from the measuring barrier.

The first experiment with our volatile spreading solvent was to determine the spreading force as a function of distance of the drop deployment site from the barrier as shown in Figure 4.6. Surprisingly, despite a wave of what might be assumed to be the spreading solvent rapidly traversing the length of the trough, the balance did not detect any significant signal until the dripping point was approximately 4 cm from the barrier. This is in line with the phenomenon reported by Burdon that when a drop of a spreading oil is placed on a talc dusted water surface, the talc is not moved until the spreading front actually reaches it. [56] As the distance was decreased below 5 cm we began to observe a measurable force acting on the float. The spreading pressure of the pure solvent increased as the distance between the dripping position and floating barrier decreases. At larger distances, it was likely that the solvent evaporates before the spreading front reaches the float.

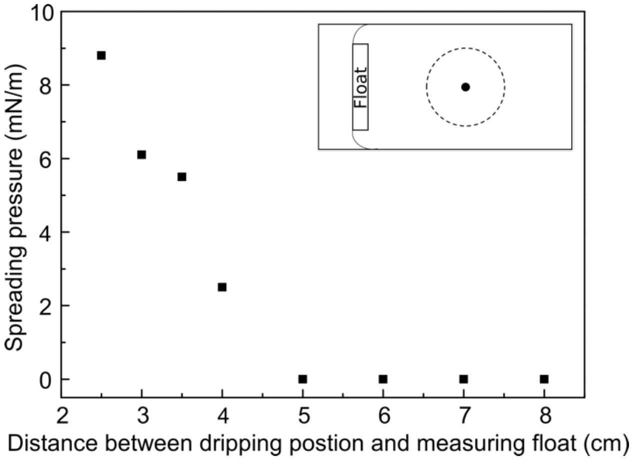

Figure 4.6 Position-dependent of spreading pressure measurement of pure solvent: A mixture of ethanol and DCE (v:v=1:13), our spreading solvent in GO deposition, was used as the solvent. The inset shows the arrangement of the dripping position and measuring float.

4.2.3 Film formation under Brewster angle microscope

In §3.2.3, we observed edge-to-edge aggregation of GO sheets as well as film densification in the deposition by using BAM. In the dilute condition (0.00625 mg/mL), we observed that the space between the GO sheets decreased as more material was added until the film was near full density at the end of the deposition. We also observed that the films were densified to a similar extent regardless of the initial arrangement of the sheets during the repetitive dripping process. In the next section, we investigate the effect of solvent spreading on the film densification by measuring the force transferred to the float by the GO film during the spreading process.

4.2.4 Spreading pressure measurement during repetitive dripping deposition of GO monolayers

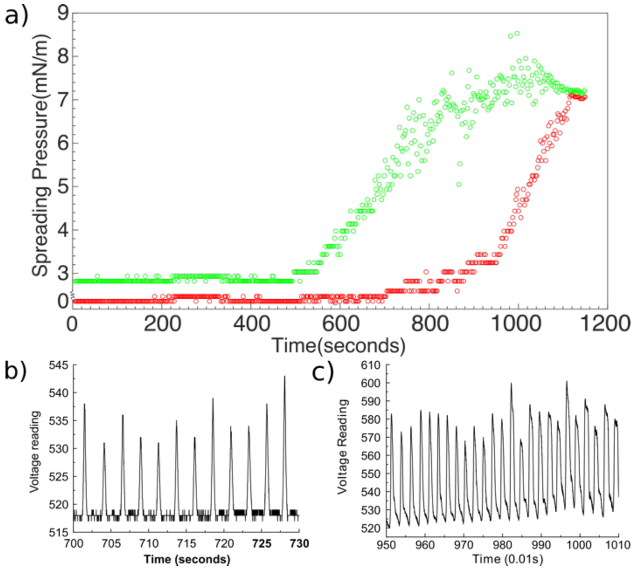

Figure 4.7 Spreading pressure measurement of GO deposition at the concentration of 0.025 mg/mL: a plot of spreading pressure changes with time (a). Voltage reading vs. time from 700 to 730 seconds (b) and from 950 to 1010 seconds (c) when no change and an increase happens respectively in the baseline value between each spreading. Note that spreading pressure in (a) was converted from voltage reading values according to corresponding calibration curve.

A plot of the surface pressure and baseline changes as a function of time during the deposition of a GO suspension at a concentration of 0.025 mg/mL is shown in Figure 4.7a. No significant measurable force was transferred to the barrier in the first 540 seconds. This is likely because most of the GO sheets were accumulating between the spreading front and floating barrier – as was observed during *in situ* BAM. Detectable peaks in the output spreading pressure were observed as each droplet spread at the water surface after 540 seconds. From the BAM imaging and our LSSA measurements, we know that the film should, at this point, extend ~4.5 cm from the barrier and thus ~4 cm from the dripping position. Therefore, the fact that we measured a spreading pressure at this time in the process is congruent with the dispersion spreading front just touching the growing film and transmitting the force to the floating barrier. Between 500 and 1000 seconds, as more GO sheets were added to the trough, and the film grew towards the center, the measured spreading pressure (green circles) increases continuously. As for the baseline values (red circles), Figure 4.7(b-c) shows the typical measuring results of spreading during continuously dripping in the time period of 700-730s and 950-1000s respectively. During the initial stages of the solvent spreading front touching the GO film, the spreading pressure was able to drop back to the baseline value as the pressure dissipated due to solvent evaporation and relaxation of the film before the next drop was deployed (Figure 4.7b). However, as more material was added, we observed an increase in the baseline value, as shown in Figure 4.7c, at the later stages of deposition (800s – 1100s). The increase in baseline values is indicative of the increase in surface pressure caused by the densely tiled GO film. The early stage of this increase is likely due to GO 'bridges' that form at the growth front from both sides of the dripping position merging at the middle. These 'bridges' prevented the film from being 'relaxed'. However, nearer the end of deposition, this increase is more likely related to remaining solvent due to the slower evaporation rate caused by the decrease in spreading area. Therefore, the continuous increase of baseline value indicates the densification of GO film as its surface pressure increased during deposition. Near the end of deposition, the baseline and surface pressure value nearly merged to the same value and at the same time the solvent could no longer spread – forming a thick lens which sat at the interface. We measured a surface pressure of the lens to be approximately 7.1 mN/m.

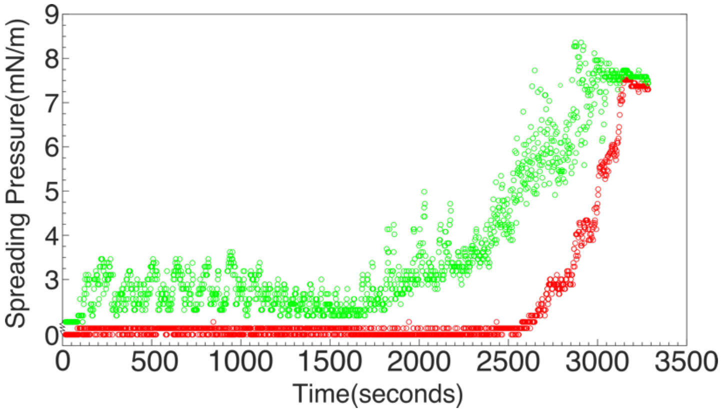

Figure 4.8 Spreading pressure measurement of GO deposition at the concentration of 0.00625 mg/mL.

The spreading pressure during deposition from a more dilute dispersion of GO is shown in Figure 4.8. The increasing trend in spreading pressure and baseline value was also observed here. However, in the dilute dispersion (0.00625 mg/mL) condition, significant changes in spreading pressure were detected (~3 mN/m) at an earlier stage, while no detectable change was obtained in the high concentration case over this range. This could be explained by the observation of the repulsive network of branched aggregates by BAM at low concentration as we discussed in §3.2.3. The network was observed to be more repulsive and may be able to transmit a force to the barrier and expand it again to be hit by the next spreading drop. In addition, compared to the high concentration case, we observed a sharper increase in the baseline values. To explain this difference, we can consider the lateral pressure from the spreading and evaporation as a movable barrier which is able to repeatedly compress and expand the GO films. By using traditional LB trough in which the barrier is moving smoothly, the compression-decompression isotherm graphs at the concentrations of 0.00625 mg/mL and 0.025 mg/mL are obtained and shown in Figure 3.5 and 4.9 respectively. An obvious hysteresis phenomenon is observed in high concentration case where expansion causes a sudden drop in the surface pressure. In contrast, the dilute deposition condition reveals a more reversible compression-expansion cycle suggesting some long range repulsion between the sheets. Therefore, compared to the high concentration case, more surface pressure would retain in the film between the time of the evaporation of last droplet and the spreading of the next one, leading to a sharper increase in baseline. At the end of the deposition, we measured the surface pressure of the lens to be 7.7 mN/m.

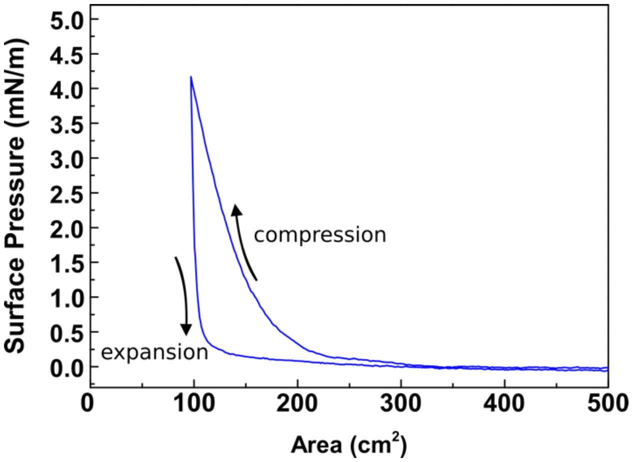

Figure 4.9 *Π-A* isotherms compression-expansion cycle at GO concentration of 0.025mg/mL

As the deposition approached its end, the surface pressure achieved a certain value against which the spreading pressure of the solvent could no longer spread. This value, the spreading pressure of solvent in a spreading circle area of radius 2.5-3 cm, is measured as 7.1 and 7.7 mN/m in high and low concentration case respectively. As no evaporation occurs in the end, this value should be equal to the spreading coefficient of the solvent. The spreading coefficient of pure DCE can be obtained by subtracting water surface tension (72.5mN/m) with the sum of the surface tension of pure DCE (32.23 mN/m [75]) and the interfacial tension of water and DCE (28.2 mN/m[76]). The result is 12.1 mN/m. We also know that the spreading coefficient of ethanol on water surface is 50.4 mN/m[77], which is much higher than the value of DCE. Therefore, by adding the ethanol, the spreading coefficient of our spreading solvent is likely to be a number a bit larger than 12.1 mN/m. However, the spreading pressure of the lens we measured is no larger than 7.7 mN/m. This difference could be due to the complexity of the contact among spreading solvent, water surface as well as GO film at the end of the deposition.

Only a few other report in the literature have attempted to measure the spreading pressure of volatile solvents. Among all these works, Transue *et al.* first used a monolayer of stearic acid at the air-water interface to provide an initial surface pressure.[64] Adding the volatile liquid to the trough acted to compress the lipid layer against the barrier for which the spreading pressure was transmitted and estimated. This experiment is similar to what might be occurring during out GO deposition process where the spreading solvent is compressing the repulsive or attractive GO film. When spreading occurs, the gradient of interfacial tension at the spreading front drags the molecules from the source moving outwards and the force could acting on the film when its within effective distance. In a typical LB assembly of GO monolayers, it is reported that GO sheets could remain flat and separated without inducing winkles and overlaps even if the surface pressure increased to ~14 mN/m [1]. The maximum spreading pressure we measure at 2.5 cm away from the float is less than 10 mN/m and thus the solvent spreading shouldn’t damage the GO monolayer films in our deposition which is the case we observed in the resulting film shown in Figure 3.8.

4.3 Conclusions

In this chapter, we discuss the development of Langmuir-Adam balance and validate the instrument by measuring the equilibrium surface pressure of stearic acid. We then studied the spreading of the DCE/ethanol solvent and found out that the spreading pressure increased as the distance between the float and dripping position decreased. By processing GO deposition at different concentration on the trough equipped with the Langmuir-Adam balance, we came to the conclusions that (i) the spreading pressure varies along the diameter of the spreading area, increasing to 7-8 mN/m as the spreading front grows closer to the point of injection. No significant force (< 2 mN/m) could be detected from a spreading radius beyond 5 cm from the dripping position. (ii) Once the spreading front could reach the floating materials, solvent spreading exerted a measurable force on the objects. (iii) Our results suggest that the force of densification can be manipulated by controlling either the distance from the dripping position and/or by using solvent/solvent mixtures with varying spreading pressures and volatilities in future work.

5 Langmuir Film of Other 2D Materials and Introduction of Continuous Coating Concepts

2D materials have drawn considerable interest due to their demonstrated performance improvements in various application especially in electronic devices.[78–80] However, the approaches to create monolayers of these 2D materials is mostly limited to the CVD process which is high cost and difficult to scale-up. In this chapter, we discuss the results of large area Langmuir film formation via repetitive dripping process of other 2D materials such as thermally exfoliated graphene oxide (TEGO) and molybdenum disulfide (MoS_2) which requires the use of suitable spreading solvents. A hybrid Langmuir film of graphene oxide and MoS_2 is also investigated. Moreover, we will introduce the concept and ability of our dripping process to be carried out continuously using TEGO films as an example which can be more easily observed by the naked eye during film growth and transfer.

5.1 Experimental

5.1.1 Thermal Reduction of Graphene Oxide

Graphene oxide powder was obtained by spray drying a GO/water dispersion (BUCHI Spray dryer B-290). The GO powder was left to dry under flowing N_2 atmosphere overnight to minimize the moisture content before thermal expansion. The dry powder was loaded into quartz tubes and thermally reduced rapidly at 1100^{o}C for 30s under argon atmosphere (Thermo Scientific).[81] This process creates a high surface area powder of rGO which can be effectively dispersed in a variety of non-aqueous solvents by tip ultrasonication.

5.1.2 MoS_2 and TEGO Spreading Suspensions for Barrier-Free Deposition

MoS_2 few-layer sheets were synthesized by chemically exfoliation of MoS_2 powder by lithium intercalation.[82,83] In a typical exfoliation procedure, 0.5 g MoS_2 powder (chemical info) was added into 7 mL 1.6 M butylithium solution in hexane (Acros Organics) in a flask and stirred for 3 days under argon atmosphere at room temperature. The resulting intercalated MoS_2 powder was collected by vacuum filtration and washed by rinsing with 50 mL of hexane twice to remove the excess of n-butylithium. Then the filter cake was transferred and exfoliated in 150 mL DI water. Both filtration and water-assisted exfoliation procedures were completed under nitrogen atmosphere. After 1 h bath sonication, 10% HCl (Sigma-Aldrich) was used to adjust the MoS_2 aqueous dispersion to pH around 2. After 12 h, the exfoliated MoS_2 aggregated and sedimented and were collected by vacuum filtration followed by a few washing steps including 5ml DI water and two times of 10 mL DMF (Sigma-Aldrich). Then, the obtained filter cake was redispersed in DMF followed by centrifugation at 2000 rpm for 30 min to remove unexfoliated flakes. The final MoS_2 spreading dispersion was prepared by mixing 4 mL of DCE with 4 mL as-prepared MoS_2 dispersion in DMF.

To prepare the TEGO spreading dispersion, 2 mg of as-prepared TEGO was mixed with 20 mL DCE followed by 30 min tip sonication. The final TEGO spreading dispersion was prepared by mixing 714 µL ethanol with 4 times diluted as prepared TEGO dispersion in DCE.

5.1.3 Continuous Coating Setup

The trough area was limited to a 7.5×11 cm^2 coating area by using a Teflon wrapped barrier. The trough was cleaned by DCE and rinsed with MilliQ water. A long strip of PET film with width of 6.5 cm was cleaned via sonication for 30 s in each solvents including ethanol, acetone and isopropanol followed by drying with air flow. A large glass piece was placed on the trough which was then filled with MilliQ water. Around 15 cm of the cleaned PET strip was placed underneath the water leaving the rest placed along the track and connected to a motor which was used to control the coating speed. Then the as-prepared TEGO suspension at a concentration of 0.1 mg/mL was repetitively dripped onto the coating area with a dripping speed of 0.13 min/mL. After 2.5 min, the continuous coating started by pulling out the PET strip at a speed of 1 cm/min. The deposition was stopped when the entire length of PET was coated.

5.1.4 Barrier-Free Langmuir Film of GO and MoS_2 Hybrid Film

The trough was first cleaned by DCE and rinsed with MilliQ water and then filled with 585 mL MilliQ water. A large glass piece was placed underneath the water as sample stages to support cleaned mica. A Teflon tape wrapped barrier was used to separate the whole trough area into a deposition area with a size of 12×17 cm^2 and the rest as clean water surface. The as-prepared MoS_2 was dripped onto the air-water interface using a clean glass syringe and Teflon tubing with inner diameter of 159 μm and outer diameter of 312 μm using a syringe pump (KD Scientific, model 230) at a rate of 0.10 mL/min. After 10 min, the floating material was switched to GO. The deposition is continued until the solvent could no longer spread. The final resulting film was deposited on arbitrary substrates by removing the subphase water.

5.1.5 Characterization of Films

Contact mode AFM was carried out on GO films deposited on atomically flat muscovite mica (SPI) substrates using NP-STT10 tips (Bruker) and a Nanoscope MultiMode AFM (Veeco).

5.2 Results and Discussion

5.2.1 Langmuir film of TEGO and MoS_2

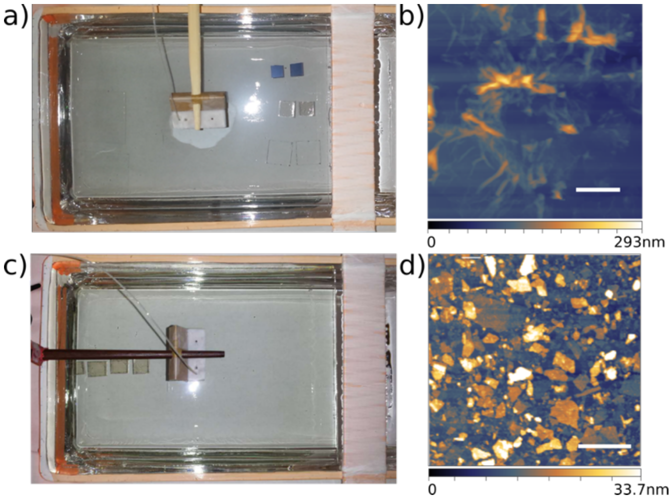

Figure 5.1 Large area Langmuir film of other 2D materials: ~204 cm^2 water surface covered with Langmuir film of TEGO (a) and MoS_2 (c) with film morphology examined by AFM shown in (b) and (d) respectively. The scar bar in (b) is 500 nm and (d) is 1 µm.

As shown in Figure 5.1, we are able to create dense, Langmuir films of other 2D materials such as thermally exfoliated graphite oxide (TEGO) and 1T-MoS_2 when these materials are dispersed in suitable spreading solvents and repetitively dripped at the air-water interface. This indicates that the film formation process may be to some extent universal for 2D nanomaterials and possibly other nanomaterial types. Conveniently, several of these materials such as TEGO and MoS_2 absorb more light and film formation can be more easily observed by the naked eye.

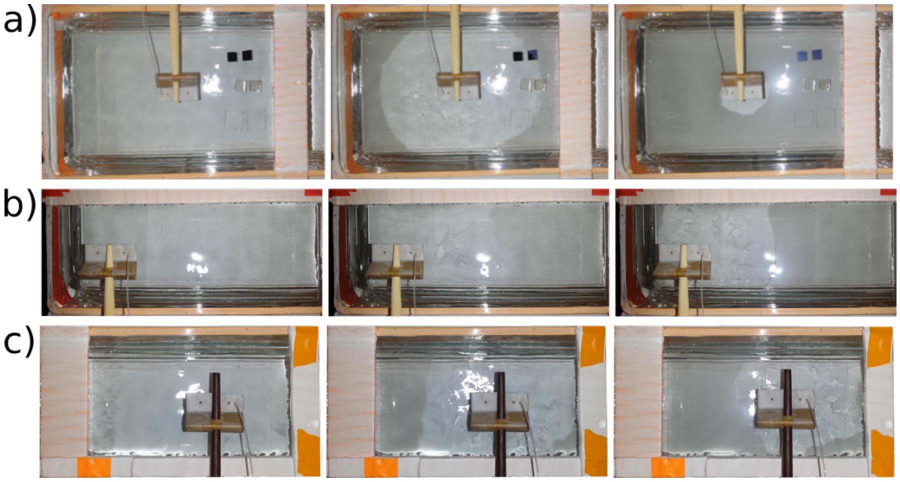

Figure 5.2 Macroscopic view of film formation of TEGO film by barrier-free at various condition: Snapshots of videos recorded through TEGO deposition by setting the dripping position at the center (a) and close to one side of the trough (b, c) from two typical concentrations: 0.025 mg/mL (a, b) and 0.1 mg/mL (c).

As shown in Figure 5.2a, TEGO films deposited from the same DCE/ethanol mixture show a similar behavior to what was observed during the spreading of the transparent GO film. In the more concentrated case (for TEGO this is ~0.1 mg/mL) we observed the formation of small islands visible by the naked eye with each drop which were pushed to the extremities of the trough by the next drop. This 2D aggregation appeared to take place during evaporation of the thin solvent film that distributes material over the air-water interface. These small islands coalesced to form larger ones, until a uniform film began to spread from the outside of the trough inwards. Then the film grew with each additional drop of dispersion until the entire trough is covered. The resulting film was found to be composed of discretely tiled sheets with a much more wrinkled morphology which is typical of TEGO[42], as the AFM image shown in Figure 5.1b.

The LSSA estimated for TEGO was found to be 300 m^2/g which is consistent with a film composed of on average ~ 8 layers of graphene if one considers the theoretical SSA of graphene to be 2675m^2/g. UV/vis absorption measurements showed ~83% transmittance of these films at 512 nm. Since the theoretical absorbance of one graphene sheet at this wavelength (2.3%) [84], these optical measurements indicate ~ 7 of layers which is in relatively good agreement with our estimate of LSSA. We achieved similar results for 1T-MoS_2 film where it was estimated that the maximum LSSA value is ~250 m^2/g. Unfortunately, 2D materials like TEGO and MoS_2 are more challenging to exfoliate compared to GO and are less uniform in terms of thickness distribution.

5.2.2 Continuous Coating of TEGO Film

The directionality of the film growth (from the outside-in) lead us to conclude that the film formation mechanism observed for these various materials could be translated into a continuous coating bath process. As shown in Figure 5.2(b-c), by changing the position of the dripping closer to one edge, we could selectively assemble the film from one side of the trough or another. By placing a long piece of clean PET film beneath the sub-phase water, and withdrawing the film at a similar velocity to that of the growing front, we were able to form uniform coatings over arbitrary lengths. A small section is shown in Figure 5.3a. A dimension of 6.5 x 14 cm^2 TEGO coated PET (Figure 5.3b) could easily be coated in this way. This demonstrates the potential utility of this approach towards creating inexpensive coatings compatible with continuous, roll-to-roll processing. While it was shown recently that roll-to-roll transfer from an LB trough is possible, these researchers required mechanical barriers to compress the film which would only allow them to transfer a length of material similar to that of the length of the compressed film.[25] In this work, the film can, in principle, be transferred continuously once suitable feedback controls are developed.

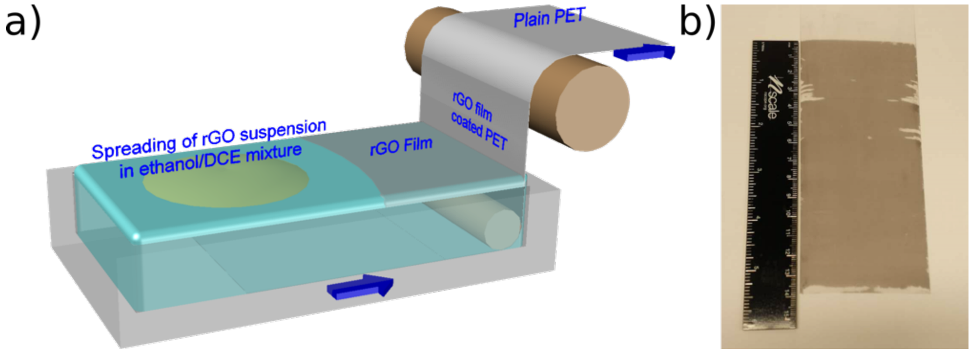

Figure 5.3 Continuous coating experiment: Schematic illustration of continuous coating setup and operation (a) as well as resulting PET sample coated with TEGO film in a dimension of 6.5 cm by 14 cm (b).

5.2.3 Hybrid Langmuir film of GO and MoS_2

The resulting film of hybrid Langmuir film of GO and MoS_2 was transferred onto a large glass piece and several mica substrates. During the deposition, we first observed that aggregated MoS_2 sheets gathered at the edges and formed liquid-phase-like film and then turned into solid-like film. When the spreading dispersion was switched to GO, the spreading of GO suspension broke the dense film into small islands and induced turbulent at the boundary between MoS_2 covered and uncovered region. As more GO was added, the growing front passed the mixing region and both the MoS_2 region and mixing region became solid. The large glass piece coated with the resulting film is shown in Figure 5.4a, from the edges to the center, the dark green region is coved by densely packed MoS_2 film and the AFM image is shown in Figure 5.4b. Then a color gradient region is observed for the hybrid film as the film transitioned from MoS_2 to a densely tiled GO monolayer. Interestingly, in the mixing region, instead of an apparent boundary between two films, we observed a mixing pattern in which each big GO single sheet were surrounded by continuously linked MoS_2 sheets (Figure 5.4c). By using heat treatment, GO can be reduced to conductive material and chemical exfoliated MoS_2 will be transferred from 1T phase to 2H phase which exhibits semiconducting properties. Therefore, this resulting hybrid film could potentially be a candidate material in applications such as transparent photodetectors or electroluminescent displays.

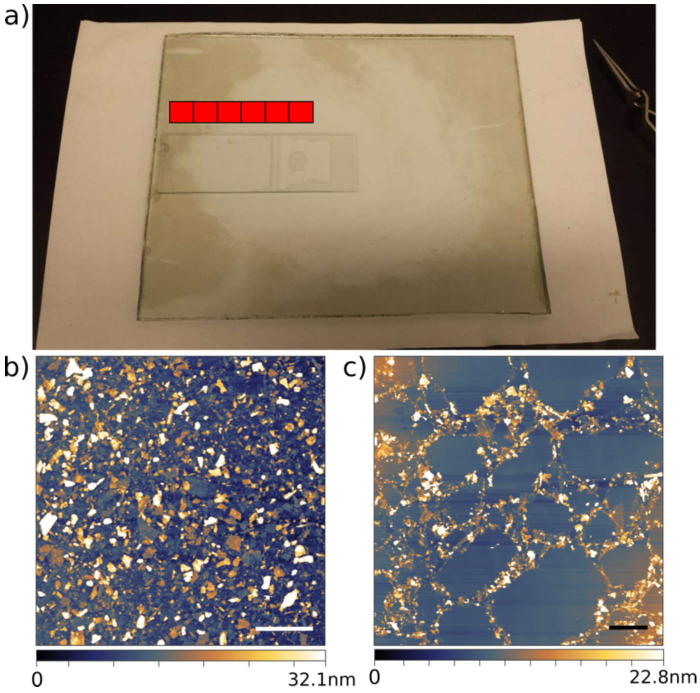

Figure 5.4 Hybrid Langmuir film of GO and MoS_2. The big glass coated with resulting hybrid film(a). Note that the dark area is covered by MoS_2 film, the center transparent area is coved by GO film and the area in between is hybrid film. The red blocks represent the spots that mica substrates were placed. AFM images of the first and third mica substrate, from the left to the right is shown in b and c respectively. The scale bar in b and c is 2 µm.

5.3 Conclusions

While analysis in previous chapters focused mostly on GO, as this material can be exfoliated into nearly 100% single layers, in this chapter we demonstrated that large area coatings of other 2D Langmuir films grown by repetitive dripping can be achieved such as for thermally exfoliated graphene oxide (TEGO) and molybdenum disulfide (MoS_2) as long as suitable spreading solvents are used. By modifying the position at which the spreading dispersion is introduced, we demonstrated that the densely-tiled network can be grown continuously while, at the same time, withdrawing and coating a flexible substrate. These results also demonstrated the proof-of-concept for continuous roll-to-roll transfer of graphene and other 2D nanomaterials onto arbitrary substrates which uses nothing more than a water bath and a syringe pump.

6 rGO Films as a Passivation Layer for Ag Nanowire Transparent Electrodes

Silver nanowire (AgNW) electrodes have been considered as a promising candidate to replace conventional transparent conductive oxides, such as indium tin oxide (ITO) films, in the applications of touch screens, solar cells and organic light emitting diodes (OLEDs). They exhibit transparency and conductivity comparable to ITO films[85] but are cheaper, as Ag is more abundant than indium, and they can be deposited onto flexible substrates. However, the long-term instability of AgNW electrodes limits their performance in applications like solar cells and OLEDs which require long-term periods of high current flow. Current flow generates heat through Joule heating and thus accelerates degradation of the nanowires through both chemical and thermal routes. However, this can be resolved by coating the electrode with a passivation layer, a uniform thin coating to protect electrodes from degrading. Single-layer CVD graphene film has been demonstrated to prevent AgNW electrodes from degrading, and at the same time AgNW electrodes are able to retain high conductivity as well as high transparency as CVD single layer graphene provides high uniformity in density and thickness (single-layer).[86] However, the high cost, limited choices of substrates and error-prone transfer of CVD process limits this process in the development to large-scale fabrication. On the other hand, our GO monolayer offers high uniformity in film thickness and sheets density and could serve as a potential alternative for a passivation layer for AgNWs. Therefore, in this chapter, I summarized my contributions to our collaborative work with Dr. Irene Goldthorpe's research group on the application of our reduced graphene oxide (rGO) monolayers as a passivation layer to prevent silver nanowires electrode from degrading under extended current flow. An annealing study as well as surface temperature mapping under current flow were investigated on silver nanowires with and without rGO films as protective layers.

6.1 Experimental

6.1.1 Fabrication of rGO Monolayers Coated Ag Nanowire Electrodes

The AgNW/PET samples were prepared through collaboration work with Dr. Goldthorpe's research group. [65] The GO monolayer-coated AgNW/PET samples were prepared by depositing our Langmuir GO film on AgNW/PET samples. The resulting samples were dried in a vacuum oven at 60 ºC for 1 h to remove adsorbed water. A 50 mM solution of $NaBH_4$ (Fisher Scientific) in water (pH adjusted to 10 using NaOH) was heated to 50 ºC.[66] Coated samples were immersed in this solution for 15 min, followed by rinsing with DI water. The resulting chemically reduced films were dried in a vacuum oven at 60 ºC for 1 h.

6.1.2 Film Characterization

An infrared (IR) camera (FLIR SC7000) was utilized to map the distribution of spatial temperature over the electrode area while a constant current of 20 mA/cm is applied on the electrode. The constant current is provided by a DC power supply. The IR camera consist of an indium-antimony detector equipped with a focal plane array featuring 81,920 pixels (matrix 320 x 256). It is capable of performing simultaneous measurement at all 81,920 spots by the snapshot mode. A spatial resolution around 250 µm x 250 μm^2 per pixel is obtained. A thin layer of black paint was deposited over the back of the samples so as to inhibit reflection. The calibration of IR camera was processed before each measurement by measuring the reference samples through each pixel at several temperatures. Note that the smallest detectable area (pixel resolution) of this IR camera is 200 µm x 200 µm which corresponds to an area with more than one hundred nanowires. Therefore, the temperature of individual nanowires cannot be detected.

6.2 Results and Discussion

6.2.1 Annealing study

To demonstrate the utility of the uniform, large-area films of GO produced by this method, we first studied their use as transparent, conductive, blocking layers to protect Ag nanowires (AgNW) transparent conductors from degrading under annealing condition. As shown in Figure 3.9e, GO monolayers were deposited onto 2 x 4 cm^2 PET substrates pre-coated with AgNW and then chemically reduced. Both the AgNW and AgNW-rGO electrodes were annealed at 70 °C in air for 14 days. After six days, the sheet resistance of the AgNW electrode increased by 180 times compared to the initial sheet resistance (R_0), as shown in Fig 6.1a, whereas the sheet resistance of the AgN-rGO electrode increased by only 1.5 times after 14 days. The morphology changes of AgNW electrodes with or without rGO protection after annealing was also investigated by SEM. After annealing at 70 °C for 3 days, apparent defects, shown as bright spots, were observed on AgNW electrodes (Figure 6.1b) while no obvious changes occurred on AgNW-rGO electrodes (Figure 6.1c). The transparency of AgNW-rGO electrodes was reduced by only ~2-3% and the extended lifetime under heating was found to be nearly the same as what was achieved when CVD grown graphene was used as a protective layer [86] which is more expensive and difficult to transfer. Therefore, these results indicate that our rGO single layer was able to effectively prevent AgNW electrodes from degrading under annealing condition without sacrificing their original high transparency.

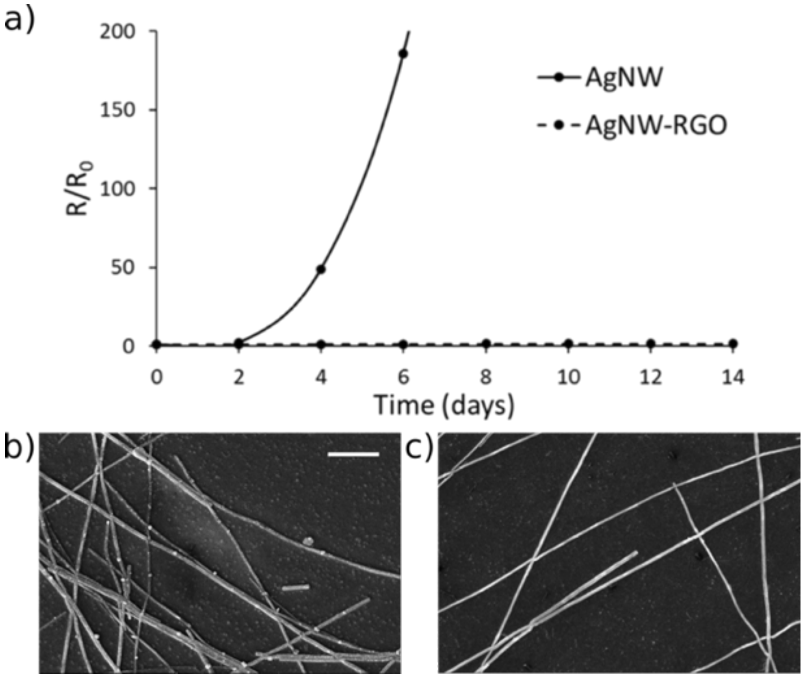

Figure 6.1 Annealing studies on AgNW and rGO coated AgNW electrodes: Sheet resistance changes of electrodes w/o a rGO layer protection as a function of annealing time at 70 °C in air (a). SEM images after 3 days annealing at 70 °C in air of AgNW (b) and rGO-coated AgNW (c). The scar bar in b, which is 2 µm is also valid in c.

6.2.2 Surface temperature distribution under current flow

As shown in Figure 6.2, surface temperature profiles of the ITO, AgNW, and rGO coated films were obtained after 10 s current flow was applied and after steady state was reached (60 s). The temperature changes on conductive surface was generally due to Joule heating, given by I^2R where I represents current and R represents resistance. As shown in Figure 6.2a-c, the temperature distributed uniformly across the film in the case of ITO and rGO-protected film, while local hot spots were observed with unprotected AgNW electrodes. Note that all the conductive films were under the same amount of current. This difference was pronounced in the 3D temperature profile (Figure 6.2c,f,i). Compared to bare AgNW electrode, the protection of rGO monolayer resulted in a uniform temperature distribution over the entire AgNW electrodes (Figure 6.2g-i). This indicate that rGO passivation layer is capable of smoothing out the temperature variation within the NW film achieving comparable uniformity to commercial ITO electrodes. This could be attributed to the high thermal conductivity of the rGO (> 1000 W/m·K) compared to air (0.024 W/m·K) and the plastic substrate (0.23 W/m·K). This result suggests that the GO monolayer prepared by our barrier-free deposition provides high uniformity in terms of thickness and density which is able to distribute heat more evenly across the surface to prevent the electrodes from degrading under current.

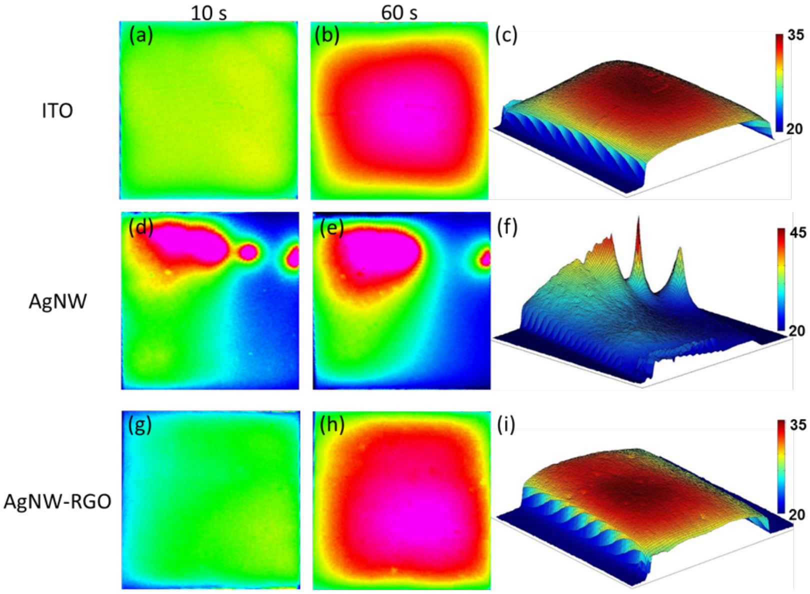

Figure 6.2 Temperature profiles of electrodes, measured using a thermal imaging camera. Surface temperature of ITO (a, b), 3D temperature profile of ITO after 60 s (c). Surface temperature of the AgNW electrodes (d, e), 3D temperature profile of the AgNW electrodes after 10s (f). Surface temperature of the AgNW-rGO electrodes (g, h), 3D temperature profile of the AgNW-rGO electrode after 60 s (i). Note that 20 mA/cm of current was constantly flowed in the direction of top to bottom.

6.3 Conclusions

In this chapter, we demonstrated that rGO single-layer films can be coated on AgNW electrodes in a large scale by first depositing our GO monolayers and then reducing these films by a chemical reduction approach. Moreover, this uniform rGO passivation layer was successfully served as a protecting layer for AgNW transparent electrodes, which could be widely applied as a thin barrier to prevent other environmentally-sensitive materials from degrading.

7 Conclusions and Future Work

7.1 Summary of Main Conclusions

In this thesis work, we achieved high yield transfer of GO single layers and the yield is not sensitive to sheet diameter by replacing the traditional spreading solvent with a mixture of ethanol and DCE (v:v=1:13) which is highly immiscible with water. While we observed a repulsive network of floating graphene oxide under dilute conditions, we found out that more concentrated conditions resulted in densely tiled islands of edge-to-edge associated sheets. Upon repetitive dripping these islands grew and coalesced to form a uniform monolayer over the entire water trough surface – a phenomena that allowed us to coat large-area substrates and measure transfer efficiencies as high as 800 m^2/(g GO). The custom-made Langmuir-Adam balance allowed us to measure the lateral pressure of solvent spreading and the results suggested that the spreading pressure varies along the diameter of the spreading area, but no significant force was exerted on the film until the growth of film reached the spreading front. Therefore, it was possible to control the force acting on the film by tuning the distance from dripping position to vary the density in the resulting film. Furthermore, by modifying the position at which the spreading dispersion is introduced, we demonstrated that the densely-tiled network could be grown continuously while, at the same time, withdrawing and coating a flexible substrate. While our analysis focused mostly on graphene oxide, as these can be exfoliated into nearly 100% single layers, we also demonstrated that the film densification phenomena was generally observed for a variety of other 2D nanomaterials such as thermally exfoliated graphene oxide (TEGO) and molybdenum disulfide (MoS_2) as long as suitable spreading solvents are used. These results demonstrated the proof-of-concept for continuous roll-to-roll transfer of graphene and other 2D nanomaterials onto arbitrary substrates which uses nothing more than a water bath and a syringe pump. While this approach may lead to a multitude of practical applications, we demonstrated the utility of transferred graphene oxide monolayer films as transparent, conducting blocking layers capable of significantly extending the lifetime of AgNW electrodes-based transparent conductors.

7.2 Future Directions

7.2.1 Improving the sensitivity of Langmuir-Adam balance

So far the balance shows good sensitivity in the range of 10-20 mN/m. However, it turns out that the measuring result we obtained in GO deposition is no larger than 10 mN/m. Therefore, we can potentially shift the detection range below 10 mN/m by changing the photodetector with high sensitivity or change the float to one made by a lighter material.

7.2.2 Extending to more 2D materials

Since we demonstrated that our barrier-free deposition approach can be applied to other 2D materials such as MoS_2 and TEGO besides GO. We could potentially extend this approach to produce large area Langmuir films of other 2D materials as long as we find appropriate spreading solvents and these materials are stable in water.

7.2.3 Developing the roll-to-roll setup

In my thesis work, I described the concept of a continuous coating bath. In the future, we should be able to set up the roll-to-roll system to achieve large-scale fabrication. In addition, according to the conclusion we obtained in §4, we will potentially be able to control the density of the resulting film by either the distance from the dripping position and/or by using solvent/solvent mixtures with varying spreading pressures and volatilities.

7.2.4 Investigating more applications

Once we are able to have good control on the resulting film over various 2D materials, we could easily build up units with heterostructure of different 2D materials by layer-by-layer deposition. One potential unit would be a heterostructure of rGO and MoS_2 which could be further doped to achieve desired electrical properties and applied in heterostructure transparent solar cells.

References

(1) Cote, L. J.; Kim, F.; Huang, J. Langmuir−Blodgett Assembly of Graphite Oxide Single Layers. *J. Am. Chem. Soc.* **2009**, *131* (3), 1043–1049.

(2) Zheng, Q.; Zhang, B.; Lin, X.; Shen, X.; Yousefi, N.; Huang, Z. D.; Li, Z.; Kim, J. K. Highly Transparent and Conducting Ultralarge Graphene Oxide / Single-Walled Carbon Nanotube Hybrid Films Produced by Langmuir-Blodgett Assembly. *J. Mater. Chem.* **2012**, *22* (48), 25072.

(3) Jia, B.; Zou, L. Langmuir–Blodgett Assembly of Sulphonated Graphene Nanosheets into Single- and Multi-Layered Thin Films. *Chem. Phys. Lett.* **2013**, *568–569*, 101–105.

(4) Mangadlao, J. D.; Santos, C. M.; Felipe, M. J. L.; de Leon, a C. C.; Rodrigues, D. F.; Advincula, R. C. On the Antibacterial Mechanism of Graphene Oxide (GO) Langmuir–Blodgett Films. *Chem. Commun.* **2015**, *51* (14), 2886–2889.

(5) Li, X.; Zhang, G.; Bai, X.; Sun, X.; Wang, X.; Wang, E.; Dai, H. Highly Conducting Graphene Sheets and Langmuir-Blodgett Films. *Nat. Nanotechnol.* **2008**, *3* (9), 538–542.

(6) Lin, X.; Jia, J.; Yousefi, N.; Shen, X.; Kim, J.-K. Excellent Optoelectrical Properties of Graphene Oxide Thin Films Deposited on a Flexible Substrate by Langmuir-Blodgett Assembly. *J. Mater. Chem. C* **2013**, *1* (41), 6869–6877.

(7) Loh, K. P.; Tong, S. W.; Wu, J. Graphene and Graphene-like Molecules: Prospects in Solar Cells. *J. Am. Chem. Soc.* **2016**, *138* (4), 1095–1102.

(8) Zheng, Q.; Shi, L.; Yang, J. Langmuir-Blodgett Assembly of Ultra-Large Graphene Oxide Films for Transparent Electrodes. *Trans. Nonferrous Met. Soc. China* **2012**, *22* (10), 2504–2511.

(9) Kim, K. S.; Zhao, Y.; Jang, H.; Lee, S. Y.; Kim, J. M.; Kim, K. S.; Ahn, J.; Kim, P.; Choi, J.-Y.; Hong, B. H. Large-Scale Pattern Growth of Graphene Films for Stretchable Transparent Electrodes. *Nature* **2009**, *457* (7230), 706–710.

(10) Akinwande, D.; Petrone, N.; Hone, J. Two-Dimensional Flexible Nanoelectronics. *Nat. Commun.* **2014**, *5*, 5678.

(11) Bae, S.; Kim, H.; Lee, Y.; Xu, X.; Park, J.; Zheng, Y.; Balakrishnan, J.; Lei, T.; Ri Kim, H.; Song, Y. Il; et al. Roll-to-Roll Production of 30-Inch Graphene Films for Transparent Electrodes. *Nat. Nanotechnol.* **2010**, *5* (8), 574–578.

(12) Wang, X.; Xiong, Z.; Liu, Z.; Zhang, T. Exfoliation at the Liquid/air Interface to Assemble Reduced Graphene Oxide Ultrathin Films for a Flexible Noncontact Sensing Device. *Adv. Mater.* **2015**, *27* (8), 1370–1375.

(13) Eda, G.; Fanchini, G.; Chhowalla, M. Large-Area Ultrathin Films of Reduced Graphene Oxide as a Transparent and Flexible Electronic Material. *Nat. Nanotechnol.* **2008**, *3* (5), 270–274.

(14) Petersen, S.; Glyvradal, M.; Bøggild, P.; Hu, W.; Feidenhans'L, R.; Laursen, B. W. Graphene Oxide as a Monoatomic Blocking Layer. *ACS Nano* **2012**, *6* (9), 8022–8029.

(15) Panda, D.; Nandi, A.; Datta, S. K.; Saha, H.; Majumdar, S. Selective Detection of Carbon Monoxide (CO) Gas by Reduced Graphene Oxide (rGO) at Room Temperature. *RSC Adv.* **2016**, *6* (53), 47337–47348.

(16) Chen, R.; Das, S. R.; Jeong, C.; Khan, M. R.; Janes, D. B.; Alam, M. A. Co-Percolating Graphene-Wrapped Silver Nanowire Network for High Performance, Highly Stable, Transparent Conducting Electrodes. *Adv. Funct. Mater.* **2013**, *23* (41), 5150–5158.

(17) Zheng, Z.; Grünker, R.; Feng, X. Synthetic Two-Dimensional Materials: A New Paradigm of Membranes for Ultimate Separation. *Adv. Mater.* **2016**, *28* (31), 6529–6545.

(18) Nair, R. R.; Wu, H. A.; Jayaram, P. N.; Grigorieva, I. V.; Geim, A. K. Unimpeded Permeation of Water Through Helium-Leak-Tight Graphene-Based Membranes. *Science.* **2012**, *335* (6067), 442–444.

(19) Wang, S.; Wu, Y.; Zhang, N.; He, G.; Xin, Q.; Wu, X.; Wu, H.; Cao, X.; Guiver, M. D.; Jiang, Z. A Highly Permeable Graphene Oxide Membrane with Fast and Selective Transport Nanochannels for Efficient Carbon Capture. *Energy Environ. Sci.* **2016**, *9* (10), 3107–3112.

(20) Eda, G.; Lin, Y. Y.; Miller, S.; Chen, C. W.; Su, W. F.; Chhowalla, M. Transparent and Conducting Electrodes for Organic Electronics from Reduced Graphene Oxide. *Appl. Phys. Lett.* **2008**, *92* (23), 10–13.

(21) Pham, V. H.; Cuong, T. V.; Hur, S. H.; Shin, E. W.; Kim, J. S.; Chung, J. S.; Kim, E. J. Fast and Simple Fabrication of a Large Transparent Chemically-Converted Graphene Film by Spray-Coating. *Carbon N. Y.* **2010**, *48* (7), 1945–1951.

(22) Becerril, H. A.; Mao, J.; Liu, Z.; Stoltenberg, R. M.; Bao, Z.; Chen, Y. Evaluation of Solution-Processed Reduced Graphene Oxide Films as Transparent Conductors. *ACS Nano* **2008**, *2* (3), 463–470.

(23) Lee, D. W.; Hong, T.-K.; Kang, D.; Lee, J.; Heo, M.; Kim, J. Y.; Kim, B.-S.; Shin, H. S. Highly Controllable Transparent and Conducting Thin Films Using Layer-by-Layer Assembly of Oppositely Charged Reduced Graphene Oxides. *J. Mater. Chem.* **2011**, *21* (10), 3438.

(24) An, S. J.; Zhu, Y.; Lee, S. H.; Stoller, M. D.; Emilsson, T.; Park, S.; Velamakanni, A.; An, J.; Ruoff, R. S. Thin Film Fabrication and Simultaneous Anodic Reduction of Deposited Graphene Oxide Platelets by Electrophoretic Deposition. *J. Phys. Chem. Lett.* **2010**, *1* (8), 1259–1263.

(25) Parchine, M.; McGrath, J.; Bardosova, M.; Pemble, M. E. Large Area 2D and 3D Colloidal Photonic Crystals Fabricated by a Roll-to-Roll Langmuir-Blodgett Method. *Langmuir* **2016**, *32* (23), 5862–5869.

(26) Silverberg, G. J.; Pearce, P.; Vecitis, C. D. Controlling Self-Assembly of Reduced Graphene Oxide at the Air-Water Interface: Quantitative Evidence for Long-Range Attractive and Many-Body Interactions. *ACS Appl. Mater. Interfaces* **2015**, *7* (6), 3807–3815.

(27) Kim, J.; Cote, L. J.; Kim, F.; Yuan, W.; Shull, K. .; J. Huang, J. Graphene Oxide Sheets at Interfaces. *J. Am. Chem. Soc.* **2010**, *132* (14), 8180–8186.

(28) Nie, H. L.; Dou, X.; Tang, Z.; Jang, H. D.; Huang, J. High-Yield Spreading of Water-Miscible Solvents on Water for Langmuir-Blodgett Assembly. *J. Am. Chem. Soc.* **2015**, *137* (33), 10683–10688.

(29) He, P.; Sun, J.; Tian, S.; Yang, S.; Ding, S.; Ding, G.; Xie, X.; Jiang, M. Processable Aqueous Dispersions of Graphene Stabilized by Graphene Quantum Dots. *Chem. Mater.* **2015**, *27* (1), 218–226.

(30) Jalili, R.; Aboutalebi, S. H.; Esrafilzadeh, D.; Konstantinov, K.; Moulton, S. E.; Razal, J. M.; Wallace, G. G. Organic Solvent-Based Graphene Oxide Liquid Crystals: A Facile Route toward the Next Generation of Self-Assembled Layer-by-Layer Multifunctional 3D Architectures. *ACS Nano* **2013**, *7* (5), 3981–3990.

(31) Osada, Y.; Okuzaki, H.; Hori, H. Crumpled and Collapsed Conformation in Graphite Oxide Membranes. *Nature* **1992**, *355* (6357), 242–244.

(32) Gudarzi, M. M. Colloidal Stability of Graphene Oxide: Aggregation in Two Dimensions. *Langmuir*

2016, *32* (20), 5058–5068.

(33) Geim, A. K.; Novoselov, K. S. The Rise of Graphene. *Nat. Mater.* **2007**, *6* (3), 183–191.

(34) Novoselov, K. S. Electric Field Effect in Atomically Thin Carbon Films. *Science.* **2004**, *306* (5696), 666–669.

(35) Marcano, D. C.; Kosynkin, D. V.; Berlin, J. M.; Sinitskii, A.; Sun, Z.; Slesarev, A.; Alemany, L. B.; Lu, W.; Tour, J. M. Improved Synthesis of Graphene Oxide. *ACS Nano* **2010**, *4* (8), 4806–4814.

(36) Higginbotham, A. L.; Lomeda, J. R.; Morgan, A. B.; Tour, J. M. Graphite Oxide Flame-Retardant Polymer Nanocomposites. *ACS Appl. Mater. Interfaces* **2009**, *1* (10), 2256–2261.

(37) Stankovich, S.; Dikin, D. A.; Piner, R. D.; Kohlhaas, K. A.; Kleinhammes, A.; Jia, Y.; Wu, Y.; Nguyen, S. B. T.; Ruoff, R. S. Synthesis of Graphene-Based Nanosheets via Chemical Reduction of Exfoliated Graphite Oxide. *Carbon N. Y.* **2007**, *45* (7), 1558–1565.

(38) Dreyer, D. R.; Park, S.; Bielawski, C. W.; Ruoff, R. S. The Chemistry of Graphene Oxide. *Chem. Soc. Rev.* **2010**, *39* (1), 228–240.

(39) Mkhoyan, K. A.; Contryman, A. W.; Silcox, J.; Stewart, D. A.; Eda, G.; Mattevi, C.; Miller, S.; Chhowalla, M. Atomic and Electronic Structure of Graphene-Oxide. *Nano Lett.* **2009**, *9* (3), 1058–1063.

(40) Hontoria-Lucas, C.; López-Peinado, A. J.; López-González, J. de D.; Rojas-Cervantes, M. L.; Martín-Aranda, R. M. Study of Oxygen-Containing Groups in a Series of Graphite Oxides: Physical and Chemical Characterization. *Carbon N. Y.* **1995**, *33* (11), 1585–1592.

(41) Yang, D.; Velamakanni, A.; Bozoklu, G.; Park, S.; Stoller, M.; Piner, R. D.; Stankovich, S.; Jung, I.; Field, D. A.; Ventrice, C. A.; et al. Chemical Analysis of Graphene Oxide Films after Heat and Chemical Treatments by X-Ray Photoelectron and Micro-Raman Spectroscopy. *Carbon N. Y.* **2009**, *47* (1), 145–152.

(42) Pope, M. Electrochemical Double-Layer Capacitors Based on Functionalized Graphene. **2006**, *7354*.

(43) Reina, A.; Jia, X.; Ho, J.; Nezich, D.; Son, H.; Bulovic, V.; Dresselhaus, M. S.; Jing, K. Large Area, Few-Layer Graphene Films on Arbitrary Substrates by Chemical Vapor Deposition. *Nano Lett.* **2009**, *9* (1), 30–35.

(44) Li, X.; Colombo, L.; Ruoff, R. S. Synthesis of Graphene Films on Copper Foils by Chemical Vapor Deposition. *Adv. Mater.* **2016**, 6247–6252.

(45) Collier, C. P. Reversible Tuning of Silver Quantum Dot Monolayers Through the Metal-Insulator Transition. *Science.* **1997**, *277* (5334), 1978–1981.

(46) Yang, P.; Kim, F. Langmuir - Blodgett Assembly of One-Dimensional Nanostructures. *ChemPhysChem* **2002**, *3* (6), 503–506.

(47) Responsivity, H.; Cao, Y.; Wei, Z.; Liu, S.; Gan, L.; Guo, X.; Xu, W.; Steigerwald, M. L. High-Performance Langmuir – Blodgett Monolayer Transistors with. **2010**, 6319–6323.

(48) Imaizumi, Y.; Kushida, M.; Arakawa, Y.; Arai, F.; Fukuda, T. Self-Assembled Giant Carbon Nanotube Construction Using Langmuir–Blodgett Films. *Thin Solid Films* **2006**, *509* (1–2), 160–163.

(49) Cao, Q.; Han, S.; Tulevski, G. S.; Zhu, Y.; Lu, D. D.; Haensch, W. Arrays of Single-Walled Carbon Nanotubes with Full Surface Coverage for High-Performance Electronics. *Nat. Nanotechnol.* **2013**, *8* (3), 180–186.

(50) Li, X.; Zhang, L.; Wang, X.; Shimoyama, I.; Sun, X.; Seo, W.; Dai, H. Langmuir−Blodgett

Assembly of Densely Aligned Single-Walled Carbon Nanotubes from Bulk Materials. *J. Am. Chem. Soc.* **2007**, *129* (16), 4890–4891.

(51) Cote, L. J.; Kim, J.; Zhang, Z.; Sun, C.; Huang, J. Tunable Assembly of Graphene Oxide Surfactant Sheets: Wrinkles, Overlaps and Impacts on Thin Film Properties. *Soft Matter* **2010**, *6* (24), 6096.

(52) Cote, L. J.; Kim, J.; Tung, V. C.; Luo, J.; Kim, F.; Huang, J. Graphene Oxide as Surfactant Sheets. *Pure Appl. Chem.* **2010**, *83* (1), 95–110.

(53) Li, X.; Gilchrist, J. F. Large-Area Nanoparticle Films by Continuous Automated Langmuir-Blodgett Assembly and Deposition. *Langmuir* **2016**, *32* (5), 1220–1226.

(54) Botcha, V. D.; Narayanam, P. K.; Singh, G.; Talwar, S. S.; Srinivasa, R. S.; Major, S. S. Effect of Substrate and Subphase Conditions on the Surface Morphology of Graphene Oxide Sheets Prepared by Langmuir-Blodgett Technique. *Colloids Surfaces A Physicochem. Eng. Asp.* **2014**, *452* (1), 65–72.

(55) Imperiali, L.; Liao, K. H.; Clasen, C.; Fransaer, J.; MacOsko, C. W.; Vermant, J. Interfacial Rheology and Structure of Ttiled Graphene Oxide Sheets. *Langmuir* **2012**, *28* (21), 7990–8000.

(56) Burdon, R. S. *Surface Tension and the Spreading of Liquids*, 2nd Ed.; Cambridge Univeristy Press, **1949**.

(57) Huh, C.; Inoue, M.; Mason, S. Uni-Directional Spreading of One Liquid on the Surface of Another. *Can. J. Chem. Eng.* **1975**, *53*, 367–371.

(58) Davies, J. T.; Rideal, E. *Interfacial Phenomena*; Academic Press, **1963**.

(59) Dussaud, A. D.; Troian, S. M.; Dussaud, A. D.; Troian, S. M. Dynamics of Spontaneous Spreading with Evaporation on a Deep Fluid Layer Dynamics of Spontaneous Spreading with Evaporation on a Deep Fluid Layer. **2010**, *23* (1998).

(60) Jia, B.; Zou, L. Langmuir-Blodgett Assembly of Sulphonated Graphene Nanosheets into Single- and Multi-Layered Thin Films. *Chem. Phys. Lett.* **2013**, *568–569*, 101–105.

(61) Yang, Y.; Yang, X.; Yang, W.; Li, S.; Xu, J.; Jiang, Y. Ordered and Ultrathin Reduced Graphene Oxide LB Films as Hole Injection Layers for Organic Light-Emitting Diode. *Nanoscale Res. Lett.* **2014**, *9* (1), 537.

(62) Liu, Y. M.; Punckt, C.; Pope, M. A.; Gelperin, A.; Aksay, I. A. Electrochemical Sensing of Nitric Oxide with Functionalized Graphene Electrodes. *ACS Appl Mater Interfaces* **2013**, *5* (23), 12624–12630.

(63) Gaines, G. L. *Insoluble Monolayer at Liquid-Gas Interfaces*, 1st Ed.; Interscience Publisher, **1966**.

(64) Transue, L. F.; Washburn, E. R.; Kahler, F. H. The Direct Measurement of the Spreading Pressures of Volatile Organic Liquids on Water. *J. Am. Chem. Soc.* **1942**, *64* (2), 274–276.

(65) Khaligh, H. H. Silver Nanowire Transparent Electrodes: Fabrication, Characterization, and Device Integration. **2013**, 25–30.

(66) Shin, H. J.; Kim, K. K.; Benayad, A.; Yoon, S. M.; Park, H. K.; Jung, I. S.; Jin, M. H.; Jeong, H. K.; Kim, J. M.; Choi, J. Y.; et al. Efficient Reduction of Graphite Oxide by Sodium Borohydride and Its Effect on Electrical Conductance. *Adv. Funct. Mater.* **2009**, *19* (12), 1987–1992.

(67) Bradder, P.; Ling, S. K.; Wang, S.; Liu, S. Dye Adsorption on Layered Graphite Oxide. *J. Chem. Eng. Data* **2011**, *56* (1), 138–141.

(68) He, H.; Klinowski, J.; Forster, M.; Lerf, A. A New Structural Model for Graphite Oxide. *Chem. Phys. Lett.* **1998**, *287* (April), 53–56.

(69) Lerf, A.; He, H.; Forster, M.; Klinowski, J. Structure of Graphite Oxide Revisited. *J. Phys. Chem. B* **1998**, *102* (23), 4477–4482.

(70) Uhl, F. M.; Wilkie, C. A. Preparation of Nanocomposites from Styrene and Modified Graphite Oxides. *Polym. Degrad. Stab.* **2004**, *84* (2), 215–226.

(71) Stankovich, S.; Piner, R. D.; Chen, X.; Wu, N.; Nguyen, S. T.; Ruoff, R. S. Stable Aqueous Dispersions of Graphitic Nanoplatelets via the Reduction of Exfoliated Graphite Oxide in the Presence of Poly(sodium 4-Styrenesulfonate). *J. Mater. Chem.* **2006**, *16* (2), 155–158.

(72) Konkena, B.; Vasudevan, S. Understanding Aqueous Dispersibility of Graphene Oxide and Reduced Graphene Oxide through pKa Measurements. *J. Phys. Chem. Lett.* **2012**, *3* (7), 867–872.

(73) Lee, Y. L.; Liu, K. L. Relaxation Behaviors of Monolayers of Octadecylamine and Stearic Acid at the Air/water Interface. *Langmuir* **2004**, *20* (8), 3180–3187.

(74) Patil, S.; Patil, V.; Sathaye, S.; Patil, K. Facile Room Temperature Methods for Growing Ultra Thin Films of Graphene Nanosheets, Nanoparticulate Tin Oxide and Preliminary Assessment of Graphene-Tin Oxide Stacked Layered Composite Structure for Supercapacitor Application. *RSC Adv.* **2014**, *4* (8), 4094–4104.

(75) Dean, J. A. *Handbook of Chemistry.*, 15th Ed.; McGraw-Hill, inc., **1999**.

(76) Hou, B.; Laanait, N.; Yu, H.; Bu, W.; Yoon, J.; Lin, B.; Meron, M.; Luo, G.; Vanysek, P.; Schlossman, M. L. Ion Distributions at the water/1,2-Dichloroethane Interface: Potential of Mean Force Approach to Analyzing X-Ray Reflectivity and Interfacial Tension Measurements. *J. Phys. Chem. B* **2013**, *117* (17), 5365–5378.

(77) Harkins, W. D.; Feldman, A. The Spreading of Liquids and The Spreading Coefficient. *J. Am. Chem. Soc.* **1922**, *44* (12), 2666–2685.

(78) Xia, F.; Wang, H.; Xiao, D.; Dubey, M.; Ramasubramaniam, A. Two-Dimensional Material Nanophotonics. *Nat. Photonics* **2014**, *8* (12), 899–907.

(79) Wang, Q. H.; Kalantar-Zadeh, K.; Kis, A.; Coleman, J. N.; Strano, M. S. Electronics and Optoelectronics of Two-Dimensional Transition Metal Dichalcogenides. *Nat. Nanotechnol.* **2012**, *7* (11), 699–712.

(80) Service, R. F. Beyond Graphene. *Science* **2015**, *348* (6234), 490.

(81) Schniepp, H. C.; Li, J. L.; McAllister, M. J.; Sai, H.; Herrera-Alonson, M.; Adamson, D. H.; Prud'homme, R. K.; Car, R.; Seville, D. A.; Aksay, I. A. Functionalized Single Graphene Sheets Derived from Splitting Graphite Oxide. *J. Phys. Chem. B* **2006**, *110* (17), 8535–8539.

(82) Acerce, M.; Voiry, D.; Chhowalla, M. Metallic 1T Phase MoS_2 Nanosheets as Supercapacitor Electrode Materials. *Nat. Nanotechnol.* **2015**, *10* (4), 313–318.

(83) Eda, G.; Yamaguchi, H.; Voiry, D.; Fujita, T.; Chen, M.; Chhowalla, M. Photoluminescence from Chemically Exfoliated MoS_2. *Nano Lett.* **2011**, *11* (12), 5111–5116.

(84) Nair, R. R.; Blake, P.; Grigorenko, A. N.; Novoselov, K. S.; Booth, T. J.; Stauber, T.; Peres, N. M. R.; GEIM, A. K. Fine Structure Constant Defines Visual Transparency of Graphene. *Science (80-.).* **2008**, *320* (5881), 1308–1308.

(85) Song, M.; You, D. S.; Lim, K.; Park, S.; Jung, S.; Kim, C. S.; Kim, D. H.; Kim, D. G.; Kim, J. K.; Park, J.; et al. Highly Efficient and Bendable Organic Solar Cells with Solution-Processed Silver Nanowire Electrodes. *Adv. Funct. Mater.* **2013**, *23* (34), 4177–4184.

(86) Yang, S. B.; Choi, H. K.; Lee, D. S.; Choi, C. G.; Choi, S. Y.; Kim, I. D. Improved Optical Sintering Efficiency at the Contacts of Silver Nanowires Encapsulated by a Graphene Layer. *Small*

2015, *11* (11), 1293–1300.